



# Integrative genomics positions MKRN1 as a novel ribonucleoprotein within the embryonic stem cell gene regulatory network

Paul A Cassar<sup>1,2,†</sup>, Richard L Carpenedo<sup>3,†</sup>, Payman Samavarchi-Tehrani<sup>4</sup>, Jonathan B Olsen<sup>2,4</sup>, Chang Jun Park<sup>5</sup>, Wing Y Chang<sup>3</sup>, Zhaoyi Chen<sup>3,6</sup>, Chandarong Choey<sup>3</sup>, Sean Delaney<sup>3,6</sup>, Huishan Guo<sup>7</sup>, Hongbo Guo<sup>8</sup>, R Matthew Tanner<sup>3,6</sup>, Theodore J Perkins<sup>3,7</sup>, Scott A Tenenbaum<sup>9</sup>, Andrew Emili<sup>2,4,8</sup>, Jeffrey L Wrana<sup>2,4,10</sup>, Derrick Gibbings<sup>7</sup> & William L Stanford<sup>1,2,3,5,6,7,11,\*</sup>

## Abstract

In embryonic stem cells (ESCs), gene regulatory networks (GRNs) coordinate gene expression to maintain ESC identity; however, the complete repertoire of factors regulating the ESC state is not fully understood. Our previous temporal microarray analysis of ESC commitment identified the E3 ubiquitin ligase protein Makorin-1 (MKRN1) as a potential novel component of the ESC GRN. Here, using multilayered systems-level analyses, we compiled a MKRN1-centered interactome in undifferentiated ESCs at the proteomic and ribonomic level. Proteomic analyses in undifferentiated ESCs revealed that MKRN1 associates with RNA-binding proteins, and ensuing RIP-chip analysis determined that MKRN1 associates with mRNAs encoding functionally related proteins including proteins that function during cellular stress. Subsequent biological validation identified MKRN1 as a novel stress granule-resident protein, although MKRN1 is not required for stress granule formation, or survival of unstressed ESCs. Thus, our unbiased systems-level analyses support a role for the E3 ligase MKRN1 as a ribonucleoprotein within the ESC GRN.

**Keywords** embryonic stem cells; makorin-1; RNA metabolism; stress granules

**Subject Categories** Stem Cells; Systems & Computational Biology

**DOI** 10.15252/embr.201540974 | Received 7 July 2015 | Accepted 15 July 2015 |

Published online 11 August 2015

**EMBO Reports (2015) 16: 1334–1357**

## Introduction

Embryonic stem cells (ESCs) and induced pluripotent stem cells (iPSCs) are pluripotent stem cells (PSCs), which in addition to their use to analyze mammalian development are making their way into regenerative medicine trials [1,2]. ESCs are derived from the inner cell mass of the pre-implantation embryo [3–5], whereas iPSCs are reprogrammed from differentiated cell types [6–8]. Despite differences in derivation, ESCs and iPSCs possess the two defining qualities of PSCs: self-renewal and pluripotency (the ability to give rise to all cell lineages of the adult organism). When cultured in the presence of leukemia inhibitory factor (LIF) and serum, mouse ESCs (mESCs) self-renew indefinitely *in vitro*. Conversely, removal of LIF, or addition of retinoic acid (RA), promotes their exit from the self-renewal GRN. Integrative systems-level analyses have uncovered a highly convergent GRN topology that governs ESC self-renewal [9–16]. At the core of the self-renewal GRN are the transcription factors OCT4, SOX2, and NANOG, which collectively regulate gene expression to support ESC identity.

The ESC identity is defined by the cellular properties that distinguish ESCs from other somatic cell types, including pluripotency, rapid progression through a checkpoint deficient cell cycle, and a heightened intolerance to genotoxic stress [17]. In our previous GRN analysis designed to identify novel regulators of ESC fate and function, we identified *Makorin-1* (*Mkrm1*) as transcriptionally co-regulated with numerous required regulators of the ESC state [16]. Our temporal transcriptome analysis revealed that *Mkrm1* is

1 Institute of Medical Science, University of Toronto, Toronto, ON, Canada

2 Collaborative Program in Genome Biology and Bioinformatics, University of Toronto, Toronto, ON, Canada

3 Sprott Centre for Stem Cell Research, Ottawa Hospital Research Institute, Ottawa, ON, Canada

4 Department of Molecular Genetics, University of Toronto, Toronto, ON, Canada

5 Institute of Biomaterials and Biomedical Engineering, University of Toronto, Toronto, ON, Canada

6 Department of Cellular and Molecular Medicine, University of Ottawa, Ottawa, ON, Canada

7 Department of Biochemistry, Microbiology & Immunology, University of Ottawa, Ottawa, ON, Canada

8 Banting and Best Department of Medical Research, Donnelly Centre, University of Toronto, Toronto, ON, Canada

9 Colleges of Nanoscale Science & Engineering, SUNY Polytechnic Institute, Albany, NY, USA

10 Center for Systems Biology, Lunenfeld-Tanenbaum Research Institute, Mount Sinai Hospital, Toronto, ON, Canada

11 Ottawa Institute of Systems Biology, Ottawa, ON, Canada

\*Corresponding author. Tel: +1 613 737 8899 Ext. 75495; E-mail: wstanford@ohri.ca

†These authors contributed equally to this study

actively transcribed in undifferentiated ESCs and repressed early upon commitment [16]. Genomewide promoter occupancy data from both mouse and human ESCs indicate that the *Mkrn1* promoter is occupied by OCT4 [10,12]. Moreover, RNAi-mediated depletion of *Oct4* in mESCs leads to a concomitant downregulation in *Mkrn1* gene expression [16,18] further delineating *Mkrn1* as a target of OCT4 in the ESC GRN.

*Mkrn1* encodes a C<sub>3</sub>HC<sub>4</sub> RING finger protein [19], which has demonstrated E3 ubiquitin ligase activity toward various substrate proteins identified in human cancer cell lines [20–25]. Additionally, MKRN1 contains four C<sub>3</sub>H zinc finger RNA-binding domains [19] and consistent with these domains is predicted to function as a ribonucleoprotein [19,26,27]. Notwithstanding, to date a role for MKRN1 in mRNA metabolism has been overshadowed by its function as an E3 ubiquitin ligase protein. Taking into account the potential disparate functions of MKRN1 in various cell types, we sought to explore the molecular and cellular function of MKRN1 in mESCs using an unbiased systems-level strategy.

Here, we provide a comprehensive profile of the MKRN1-centered interactome in ESCs at both the proteomic and ribonomic levels. Our approach—predicated on the integration of network analyses coupled with cellular and molecular level analyses—establishes MKRN1 as a component of mRNPs in mESCs that is recruited to stress granules upon exposure to environmental stress. MKRN1 predominantly associates with proteins involved in mRNA metabolism including regulators of mRNA turnover, transport, and/or translation. MKRN1 mRNP complexes are enriched for low-abundance mRNAs encoding regulatory proteins involved in cell differentiation or apoptosis and mRNAs of secreted proteins that are destined for translation at the ER. Importantly, predictions afforded from the unbiased network analysis were tested with molecular and cellular level analyses.

## Results

### MKRN1 protein expression correlates with the undifferentiated ESC state

*Mkrn1* is widely expressed in adult mouse tissues; however, during embryogenesis, *Mkrn1* exhibits more restricted expression [19,28]. Quantitative PCR (qPCR) analysis confirmed our microarray data [16] that *Mkrn1* mRNA expression is downregulated in committed ESC populations similar to the pluripotency markers *Oct4*, *Sox2*, and *Nanog* irrespective of the mode of differentiation (–LIF or +RA) (Fig 1A). We next explored the dynamics of MKRN1 protein expression in undifferentiated and committed ESC populations by comparing MKRN1 abundance in whole-cell lysates obtained from bulk ESCs cultured in self-renewal (+LIF), or RA-induced differentiation (+RA) conditions by Western blot analysis. Following 48 and 72 h of RA-induced ESC differentiation, both MKRN1 and the surrogate self-renewal marker, OCT4, were substantially decreased (Fig 1B), indicating that both MKRN1 mRNA and protein expression are downregulated upon differentiation.

The specificity of the MKRN1 antibody used to test the dynamics of MKRN1 expression was confirmed by immunoblot analysis of MKRN1 overexpression and knockdown ESC clones. Accordingly, bands corresponding to FLAG-epitope-tagged recombinant MKRN1 protein (FLAG:MKRN1) were uniquely detected from stable MKRN1

overexpression ESC clones, while bands representing endogenous MKRN1 were visibly reduced in lysates derived from stable MKRN1 knockdown ESC clones (Fig EV1A and B). Notably, despite robust silencing of full-length MKRN1 protein expression, the self-renewal capacity of stable MKRN1 knockdown ESCs cultured in LIF and serum was not impaired (Fig EV1B and C).

### MKRN1 is preferentially expressed in the cytoplasm of OCT4-positive ESCs

MKRN1 is reportedly expressed in the nuclei and cytoplasm when transfected in various cell types [20,26,29]; thus, immunocytochemistry was performed to examine the subcellular localization of endogenous and transgenic MKRN1 in ESC populations. At steady state, endogenous MKRN1 localization was primarily cytoplasmic and was not visible in the nucleus of these cells (Figs 1C and EV1D). Similarly, transgenic FLAG:MKRN1 was also primarily visualized in the cytoplasm of cells found in ESC populations cultured in self-renewal or RA-induced differentiation conditions (Fig EV1E). Together, these results suggest a non-nuclear molecular function for MKRN1 in ESCs.

Embryonic stem cells cultured in LIF and serum grow as a heterogeneous population, where the majority of ESCs grow as colonies of OCT4-positive (OCT4<sup>+</sup>) undifferentiated cells, and a subpopulation of committed cells are distinguishable as flattened OCT4-negative (OCT4<sup>–</sup>) cells. Co-immunostaining of ESCs cultured in LIF and serum revealed that MKRN1 was most abundant in the OCT4<sup>+</sup> cells of the ESC colony, and comparatively diminished in the OCT4<sup>–</sup> cells proximal to the colonies (Fig 1C), suggesting that MKRN1 is preferentially expressed in the undifferentiated fraction of ESCs. To test whether MKRN1 is disproportionately expressed between the OCT4<sup>+</sup> and OCT4<sup>–</sup> subpopulation, the mean fluorescent intensity of MKRN1 in the OCT4<sup>+</sup> and OCT4<sup>–</sup> fraction of ESC populations cultured for 72 h in self-renewal (+LIF) or differentiation conditions (–LIF or +RA) was quantified at the single-cell level using flow cytometry. Irrespective of culture conditions, MKRN1 protein expression was significantly more abundant in the OCT4<sup>+</sup> cells than the OCT4<sup>–</sup> subpopulation (Fig 1D), demonstrating that MKRN1 expression is correlated with OCT4 expression. This correlation was further corroborated using high-content imaging analysis (Fig EV1F), thus corroborating the preferential expression of MKRN1 in OCT4<sup>+</sup> cells of the ESC cultures.

### MKRN1 is a component of a ribonucleoprotein complex in ESCs

As our hypothesis that MKRN1 functioned to regulate PSC self-renewal was incorrect, we initiated an unbiased systems approach to dissect the molecular and cellular function of MKRN1 in ESCs. Full-length MKRN1 contains structural features that are indicative of RNA-binding and E3 ubiquitin ligase activity. To identify MKRN1-associated proteins in ESCs, including putative MKRN1 E3 ligase substrate proteins, FLAG:MKRN1 was affinity purified with anti-FLAG antibodies from bulk FLAG:MKRN1 ESC lysates and purified protein was subjected to unbiased liquid chromatography and tandem mass spectrometry (LC-MS/MS). To distinguish between stable MKRN1-associated proteins and short-lived MKRN1 substrates targeted for proteasome-mediated degradation, FLAG:MKRN1 ESC populations were pre-treated with either the proteasome inhibitor

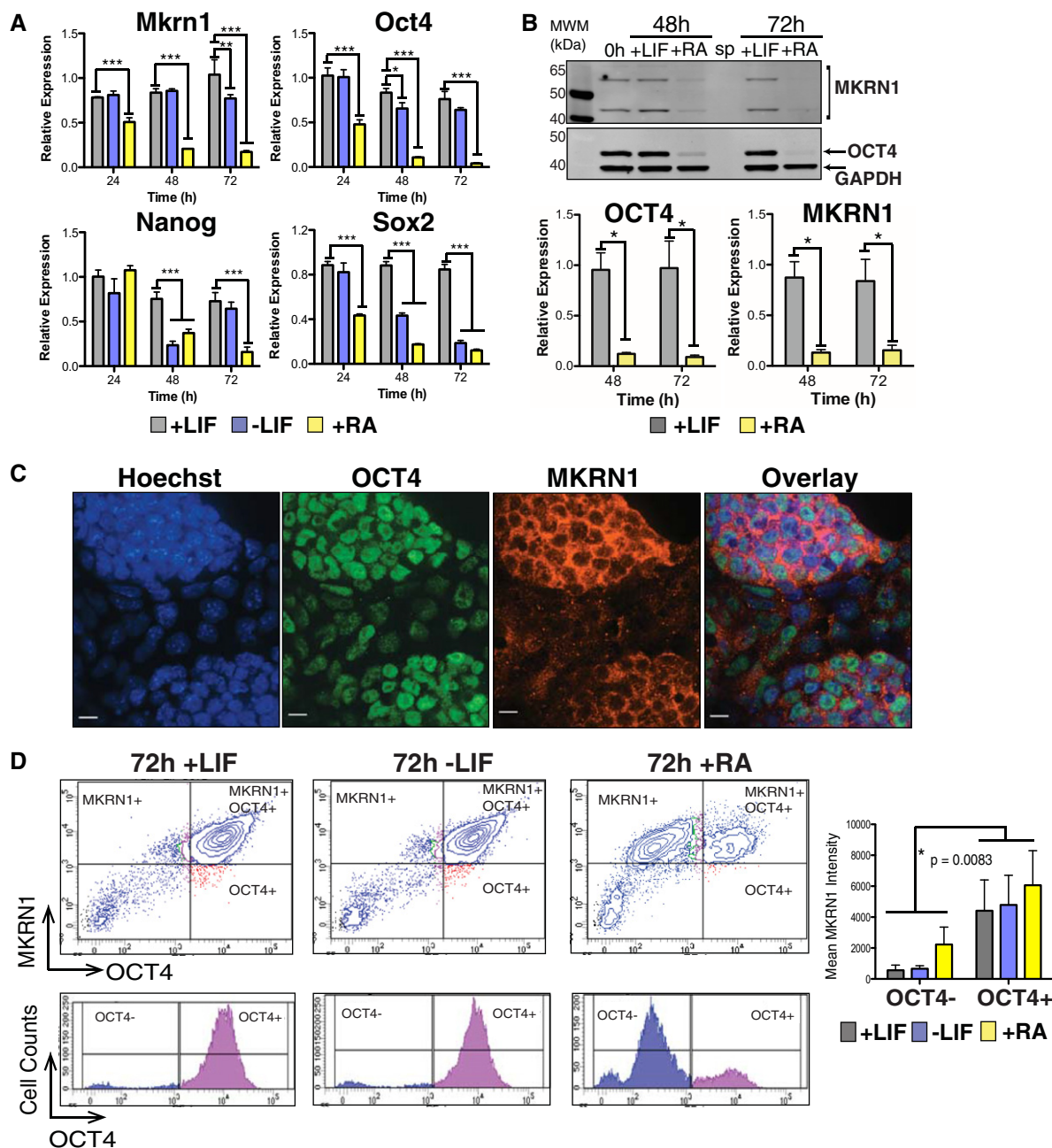


**Figure 1. MKNR1 protein expression is correlated with the undifferentiated ESC state.**

A qPCR analysis of fold change in *Mkrn1*, *Oct4*, *Nanog*, and *Sox2* mRNA expression in R1 ESCs upon differentiation induced by LIF withdrawal (-LIF) or RA treatment (+RA) relative to undifferentiated R1 ESCs collected at 0 h. Data are means  $\pm$  standard error of the mean (SEM) from three biological replicate experiments ( $*P < 0.05$ ,  $**P < 0.01$ ,  $***P < 0.0001$  vs. +LIF; two-way ANOVA).

B Quantitative immunoblot analysis of MKNR1 and OCT4 expression in R1 ESCs cultured for 48 or 72 h in self-renewal (+LIF) or differentiation conditions (+RA). The OCT4 immunoblot was first probed with anti-OCT4 antibodies and subsequently probed with anti-GAPDH antibodies. MKNR1 and OCT4 protein abundance was normalized to GAPDH and reported relative to undifferentiated R1 ESCs collected at 0 h. MKNR1 = ~53-kDa and ~42-kDa bands, OCT4 = ~45-kDa band, and GAPDH = ~37-kDa band. Data are means  $\pm$  SEM of two biological replicate experiments ( $*P < 0.05$  vs. +LIF; two-way ANOVA).

C Co-immunofluorescent staining of endogenous MKNR1 and OCT4 in R1 ESCs cultured in LIF + serum. MKNR1 is predominantly localized to the cytoplasm. Scale bars: 10  $\mu$ m.

D Intracellular flow cytometry analysis for MKNR1 and OCT4 expression from single R1 ESCs cultured in +LIF, -LIF, or +RA for 72 h. Quantile contour plots of OCT4- and MKNR1-positive/negative cells in each culture condition. Mean fluorescent intensity of MKNR1 was quantified from the OCT4<sup>+</sup> and OCT4<sup>-</sup> subpopulations in each culture condition. MKNR1 is significantly more abundant in the OCT4<sup>+</sup> subpopulation than in the OCT4<sup>-</sup> subpopulation irrespective of culture conditions. Data are means  $\pm$  SEM from three biological replicates ( $P = 0.0083$ , two-way ANOVA).

Source data are available online for this figure.

MG132, or vehicle control (DMSO) with the expectation that putative MKRN1 E3 ligase substrate proteins would be enriched in the MG132 treated immunolysates. Co-IP Western blot analysis confirmed that FLAG:MKRN1 was efficiently affinity purified exclusively from FLAG:MKRN1 ESC lysates and that the MG132 pre-treatment adequately attenuated proteasome-mediated degradation of ectopic FLAG:MKRN1 (Fig EV2A), as previously described [21,24].

LC-MS/MS analysis identified 48 proteins that were consistently enriched in FLAG:MKRN1 compared to control purifications in all biological replicate experiments (FDR < 0.05) (Table 1). Surprisingly, FLAG:MKRN1 AP-MS profiles from MG132-treated and untreated ESCs were nearly identical (Fig 2A and Table 1), suggesting that in mESCs, MKRN1 associates with proteins that are not actively destabilized by MKRN1 E3 ligase activity. Gene-enrichment analysis performed in DAVID revealed that 35 of the 48 FLAG:MKRN1-associated proteins are established RNA-binding proteins (RBPs) and/or components of ribonucleoprotein complexes ( $P = 1.1E-34$ ), and many are known to function in posttranscriptional gene regulation ( $P = 4.2E-12$ ) and/or translational control ( $P = 2.6E-06$ ) (Fig 2B). Among the list of posttranscriptional regulatory proteins were heterogeneous nuclear ribonucleoproteins (hnRNPs), PABPC1, EIF4G1, AGO2, MOV10, ELAVL1 (HuR), IGF2BP1, and YBX1. Hence, two of these established mRNA regulatory proteins, IGF2BP1 and HuR, were used as baits in reciprocal co-IP Western blot experiments to test whether endogenous MKRN1 is associated with mRNP components in ESCs. Indeed, endogenous MKRN1 was immunoprecipitated with both endogenous IGF2BP1 and HuR from bulk ESC lysates (Fig EV2B and C), suggesting that MKRN1 is found within mRNP complexes in undifferentiated ESCs, where MKRN1 is preferentially expressed. Knockdown or overexpression of MKRN1 did not affect total levels of either IGF2BP1 or HuR (Fig EV2D and E), implying that MKRN1 does not target these RBPs for ubiquitin-mediated degradation, consistent with our interpretation of the AP-MS data set; however, we cannot discount the possibility that MKRN1 ubiquitinates these proteins for alternative posttranslational regulation.

Based on the enrichment of RBPs in the FLAG:MKRN1 AP-MS data set, we sought to determine whether FLAG:MKRN1 associates with these proteins independently of RNA. Thus, following FLAG:MKRN1 immunoprecipitation from bulk ESC lysates, anti-FLAG beads were treated with RNase A (no RNase samples as a control), and purified protein was subjected to LC-MS/MS analysis on an LTQ Orbitrap Velos mass spectrometer. PABPC1, PABPC4, L1TD1, YBX1, IGF2BP1, and UPF1 remained associated with FLAG:MKRN1 in the presence of RNase; however, the association between FLAG:MKRN1 and IGF2BP1 and UPF1 was partially sensitive to RNase digestion (Fig 2C; Table EV1). Co-IP Western blot experiments from bulk FLAG:MKRN1 ESC lysates confirmed that FLAG:MKRN1 interacts with the *bona fide* mRNA-binding protein PABPC1 in a RNA-independent manner, while its associations with the mRNA-binding proteins IGF2BP1 and HuR appeared to be sensitive to RNase A treatment (Fig 2D). Thus, our unbiased proteomic analysis indicates that FLAG:MKRN1 associates with mRNA-binding proteins in RNA-independent and RNA-dependent manners and strongly suggests that MKRN1 participates in mRNA metabolism in ESCs.

The resolution and accuracy of the mass spectra generated from the LTQ Orbitrap Velos allowed individual peptide sequences of FLAG:MKRN1-associated proteins to be mined for the presence of diglycine-modified lysines (an adduct left on ubiquitinated proteins

after trypsin digestion). The presence of peptides with diglycine-modified lysines in FLAG:MKRN1 immunolysates could indicate MKRN1 target proteins that are ubiquitinated irrespective of whether proteins are targeted for proteolysis. However, this analysis failed to identify peptides with diglycine-modified lysines (unpublished observations), again suggesting that MKRN1 does not function as an E3 ubiquitin ligase in ESCs. However, additional targeted experiments would be required to completely rule out a MKRN1 ubiquitination function in mESCs.

### MKRN1 interacts with RNA in ESCs

MKRN1 contains four C<sub>3</sub>H zinc finger domains [19], which are suggestive of RNA-binding capacity. To assess the MKRN1 RNA-binding capacity in ESCs, FLAG:MKRN1 was affinity purified from bulk ESC lysates using UV cross-linking and immunoprecipitation (CLIP). Briefly, prior to lysis, ESCs were either UV irradiated to cross-link protein–RNA interactions, or left uncross-linked. FLAG:MKRN1 or FLAG:Ctrl ESC lysates were subsequently digested with optimized doses of RNase A to yield protein bound to short protected RNA fragments. Following IP with either anti-FLAG or IgG control antibodies, remaining RNA fragments were radiolabeled for detection by autoradiography. Minimal labeling was visible in uncross-linked samples and IgG control IPs from FLAG:MKRN1 ESC lysates (Fig EV2F) that should not contain covalent MKRN1–RNA complexes. In contrast, marked RNA labeling was observed in cross-linked FLAG-MKRN1 IP and titration of the RNase concentration used to pre-treat ESC lysates prior to anti-FLAG IP resulted in the expected size shifts of FLAG:MKRN1–RNA. RNase concentrations in the 1/10,000–1/30,000 range yielded a focused band indicative of FLAG:MKRN1 bound to a short fragment of RNA protected from RNase by MKRN1 (Figs 2E and EV2F). Reinforcing that this band consists of a MKRN1–RNA complex, over-exposure of the MKRN1 immunoblot allowed visualization of faint bands for MKRN1 at the mass of the labeled RNA complex (Fig 2F), consistent with detection of the 1–5% of total MKRN1 cross-linked to RNA in these types of experiments. Treatment with a lower concentration of RNase (1/100,000) caused the cross-linked MKRN1–RNA complex to smear upwards, consistent with FLAG:MKRN1 bound to longer RNAs of variable lengths. Finally, treatment with a high dose of RNase A (1/1,000) strongly reduced RNA labeling of MKRN1 complexes (Fig 2E). Cross-linked MKRN1 IPs also contained markedly more RNA labeling than anti-FLAG IP from FLAG:Ctrl lysates, although the latter contained some background RNA labeling. The residual RNA detected from FLAG:Ctrl IPs may be attributed to background binding of RBPs to FLAG beads as previously described [30], since IgG control IPs did not yield the same level of background and the intensity of the <sup>32</sup>P-labeled RNA signal was more intense from FLAG:MKRN1 IPs compared to FLAG:Ctrl IPs (Fig EV2F). Cumulatively, this suggests that MKRN1 exhibits binding capacity toward RNA, but further *in vitro* binding assays are required to confirm our hypothesis.

### MKRN1 localizes to cytosolic stress granules upon oxidative stress

Our FLAG:MKRN1 AP-MS data set revealed that in steady-state conditions, FLAG:MKRN1 is associated with known stress granule

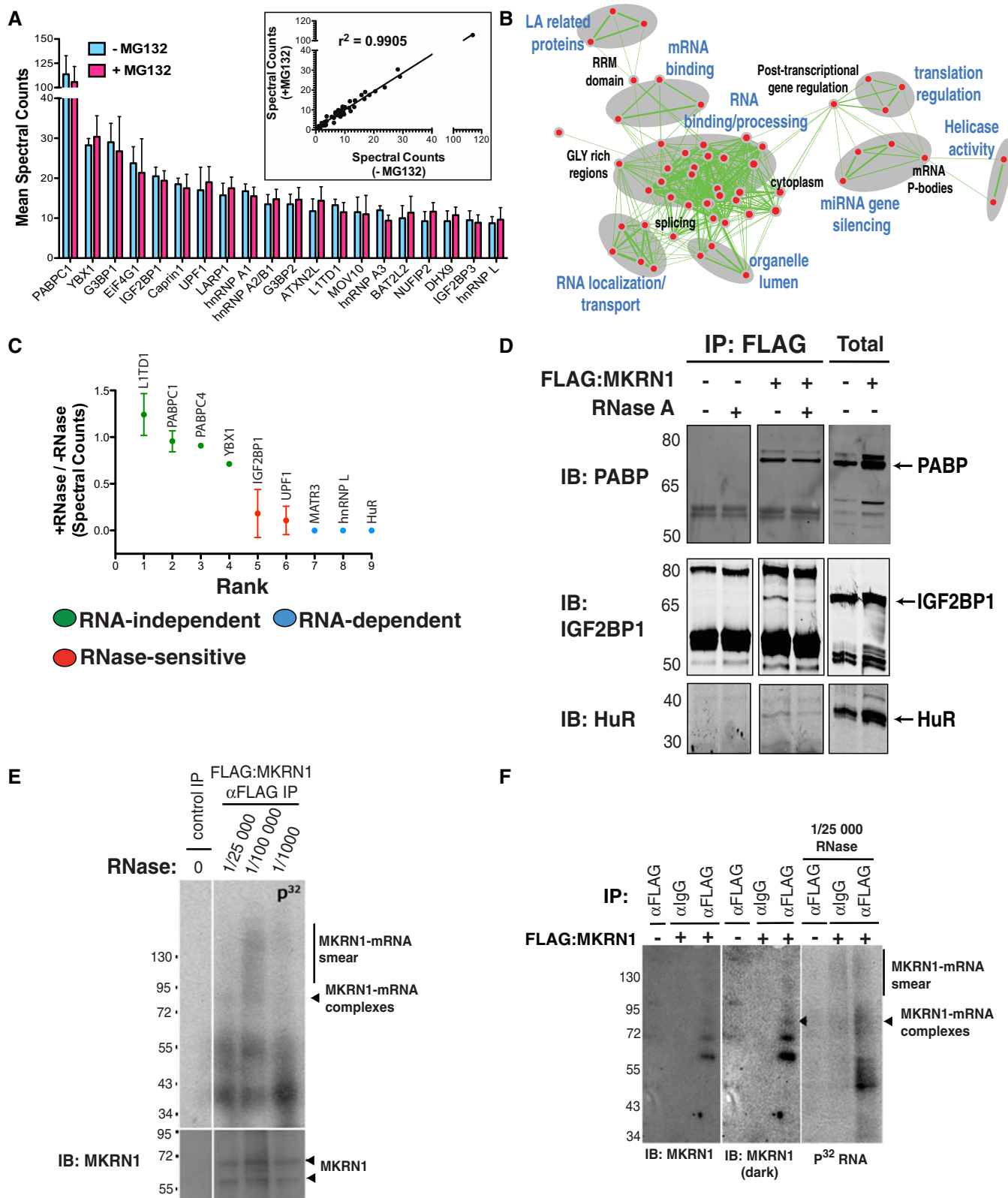


Figure 2.

(SG)-resident proteins including G3BP, CAPRIN1, HuR, PABPC1, and IGF2BP1 [31–35]. Thus, we asked whether MKRN1 is recruited to SGs upon exposure to cellular stress and, furthermore, whether

MKRN1 is required for SG assembly in ESCs. First, wild-type ESCs treated with 1 mM sodium arsenite (NaAsO<sub>2</sub>) for 1 h were co-immunostained for endogenous MKRN1 and two established SG

**Figure 2. AP-MS analysis identifies MKRN1 as a component of mRNPs in ESCs.**

- A List of the top 20 enriched proteins co-purified with FLAG:MKRN1 from MG132-treated and untreated ESC lysates ranked according to mean spectral count values. Data are means  $\pm$  SEM of three biological replicate experiments. The XY scatter plot (top right insert) indicates a strong positive correlation ( $r^2 = 0.9905$ ) in mean spectral count values for all 48 FLAG:MKRN1-associated proteins purified from MG132-treated and untreated lysates.
- B Enrichment map representation of enriched cellular processes within the FLAG:MKRN1 AP-MS data set ( $P < 0.001$ ; FDR  $< 0.1$ ). Nodes and edges are represented as described in Materials and Methods. Proteins within labeled gene sets are listed in Table EV2.
- C Proteins identified with enriched total spectral counts by LC-MS/MS from RNase A-treated and untreated FLAG:MKRN1 IPs from two biological replicate experiments. Proteins are ranked along the x-axis according to whether they are predicted to interact with MKRN1 in a RNA-independent or RNA-dependent manner.
- D Predicted RNA-independent (PABP), RNA-dependent (HuR), and RNase-sensitive (IGF2BP1) associations tested by FLAG:MKRN1 co-IP Western blots. Data are representative of two independent experiments. Note that due to limited amount of IP material, the IGF2BP1 immunoblot was re-probed with anti-HuR without stripping the blot. The ~37-kDa band corresponding to HuR was visible in FLAG:MKRN1 IPs but not control IPs.
- E Protein–RNA complexes are observed from FLAG:MKRN1 IPs, but not control IPs. Note the radioactive smear from FLAG:MKRN1 IPs treated with a low concentration of RNase (1:100,000) that is resolved to a focused band at the expected size of MKRN1–RNA complexes with moderate RNase A treatment (1:25,000) and strongly reduced with a high dose (1:1,000) of RNase A ( $n = 2$ ). CLIP data from additional RNase dilutions are provided in Fig EV2F.
- F Anti-MKRN1 immunoblot (left and center) and corresponding RNA autoradiogram (right) identify MKRN1–RNA complexes uniquely purified from FLAG:MKRN1 IPs. At the optimized RNase concentration of 1:25,000,  $^{32}$ P-labeled RNA–protein complexes purified from FLAG:MKRN1 ESC lysates resolved to a mass that corresponded to supershifted MKRN1 proteins that may reflect the RNA-bound fraction of MKRN1. Data are from CLIP samples obtained from the same experiment and are representative of two biological replicate experiments.

Source data are available online for this figure.

markers, HuR and TIAR, and examined by confocal microscopy. In untreated ESCs, MKRN1 was diffusely localized throughout the cytoplasm; however, following  $\text{NaAsO}_2$  exposure, MKRN1 was visualized in SGs co-localized with HuR and TIAR (Fig 3A, yellow arrows). Similarly, MKRN1 was also found localized in HuR-positive SGs in ESC populations undergoing thapsigargin-induced endoplasmic reticulum (ER) stress (Fig EV3A), suggesting that MKRN1 is mobilized to SGs in response to various types of environmental stress.

Next, we examined whether the manipulation of MKRN1 expression induces spontaneous SG formation in unstressed conditions. Overexpression of certain SG-resident proteins induces SG formation in the absence of stress either through the global inhibition of protein synthesis, or by obligatorily aggregating mRNP complexes into SGs [31,34,36–39]. However, SGs were not evident in unstressed pPyCAG::FLAG:MKRN1 ESC populations (Fig EV3B and C) that express twice the levels of MKRN1 protein relative to wild-type ESCs (Fig EV1A), indicating that moderate MKRN1 overexpression did not trigger spontaneous SG assembly. Importantly, antibodies that uniquely recognize endogenous MKRN1 or ectopic FLAG:MKRN1 detected MKRN1 proteins in SGs in the same MKRN1 overexpression ESC clones following  $\text{NaAsO}_2$  exposure (Fig EV3B and C), demonstrating that both ectopic FLAG:MKRN1 and endogenous MKRN1 localize to SGs upon  $\text{NaAsO}_2$ -induced stress.

To discern whether MKRN1 is required for SG assembly in uncommitted ESCs, stable MKRN1 knockdown ESC clones were stressed with  $\text{NaAsO}_2$  and SG formation was monitored in MKRN1-depleted ESCs via TIAR immunostaining. Undifferentiated MKRN1 knockdown ESCs were distinguished from committed MKRN1-negative ESCs by co-immunostaining with OCT4. MKRN1 immunostaining confirmed that endogenous MKRN1 was adequately silenced in OCT4<sup>+</sup> MKRN1 knockdown ESCs in both unstressed and  $\text{NaAsO}_2$ -stressed cells (Fig 3B). Depletion of MKRN1 did not induce the spontaneous formation of TIAR-positive SGs in unstressed ESCs, nor did it prevent the formation of SGs in stressed ESCs, as TIAR-positive SGs were visible in OCT4<sup>+</sup>/MKRN1<sup>-</sup> ESCs following  $\text{NaAsO}_2$  exposure (Fig 3B). Therefore, MKRN1 is dispensable for the nucleation of SGs in ESCs, yet its localization to SGs further corroborates MKRN1 as a novel component of mRNPs in ESCs.

### MKRN1 preferentially associates with low-abundance transcripts in ESCs, but does not globally affect the abundance of its target mRNAs

Based on our finding that MKRN1 exists within mRNP complexes, we sought to identify the subset of mRNAs selectively associated with MKRN1 in undifferentiated ESCs. Thus, FLAG:MKRN1 was affinity purified with anti-FLAG antibodies from bulk FLAG:MKRN1 ESC lysates, and co-immunoprecipitated RNA was analyzed by microarray analysis (RIP-chip). Genomewide RIP-chip analysis identified 3,192 unique transcripts that were enriched in FLAG:MKRN1 RIP samples relative to FLAG:Ctrl and isotype controls (Table EV3).

Among the enriched transcripts in FLAG:MKRN1 immunolysates were numerous lineage-commitment genes including *Cited1*, *Pitx3*, *Sox18*, *Twist1*, *Pax2*, *Pax7*, *Irx1*, *Msx2*, *Myod1*, and *Esx1*. Collectively, the mRNA and protein expression of these genes are considered repressed in ESCs through the function of various suppressive gene regulatory mechanisms [11,15,40–45]. Thus, the prevalence of transcripts encoding lineage-commitment genes in the FLAG:MKRN1 RIP data set led us to postulate that MKRN1 associates with transcripts that are expressed at low levels in undifferentiated ESC populations. To test this hypothesis, microarray expression data from undifferentiated ESC populations were mapped to the FLAG:MKRN1 RIP data set to compare the distribution in expression values of FLAG:MKRN1-associated transcripts to the overall distribution of mRNA abundance in the mESC transcriptome (Materials and Methods). Raw and normalized microarray expression values for each probe were plotted on a log-scale histogram to represent the distribution of mRNA expression in the undifferentiated mESC transcriptome. Transcripts clustered into three distinct groups when plotted across expression levels: a low bin for expression values between 1 and 100, a middle bin for expression values between 100 and 1,000, and a high bin for expression values between 1,000 and 10,000 (Fig 4A). Because raw expression values corresponding to probes in the low bin, but not the middle or high bin, were diminished following background correction (Fig 4A), transcripts populating the low bin were filtered from the FLAG:MKRN1 RIP data set to focus the analysis of transcripts in the

Table 1. FLAG:MKRN1 AP-MS data ranked according to adjusted P-values.

Bait	FLAG:MKRN1-associated proteins	FLAG:MKRN1 IP			FLAG:Ctrl IP			Adjusted P-value
		Mean UPEP	Spectral counts		Mean UPEP	Spectral counts		
			-MG132	+MG132		-MG132	+MG132	
MKRN1	IGF2BP1	16	23 21 24 14	18 18 26 15	3	3 7 1	1 5 3	7.18E-04
MKRN1	hnRNP F	6	6 7 7 8	6 5 10 8	2	0 2 2	2 0 2	8.33E-04
MKRN1	hnRNP A3	8	14 13 9 12	7 7 11 12	3	1 3 4	0 3 0	9.94E-04
MKRN1	CAPRN1	16	21 17 21 15	23 11 24 12	3	1 4 1	0 5 2	1.15E-03
MKRN1	hnRNP A1	12	20 19 16 12	12 15 22 13	5	1 5 6	0 7 4	1.15E-03
MKRN1	hnRNP U	8	12 9 10 8	6 7 10 8	3	0 3 4	0 3 0	1.24E-03
MKRN1	YBX1	18	27 31 31 24	24 21 44 32	7	2 12 5	4 15 4	1.24E-03
MKRN1	Syncrip	8	8 13 9 5	8 7 9 5	2	0 2 1	5 22 9	1.49E-03
MKRN1	L1td1	12	12 14 17 10	12 9 18 7	0	0 0 0	0 3 0	1.49E-03
MKRN1	PABPC1	64	120 117 155 63	104 89 151 79	12	10 24 11	5 22 9	1.49E-03
MKRN1	RBMXRT	4	5 5 3 2	5 3 3 6	1	0 0 1	0 0 0	1.49E-03
MKRN1	ELAVL1	8	5 9 7 6	9 4 11 8	1	0 0 0	0 1 0	1.53E-03
MKRN1	hnRNP A2/B1	11	18 17 11 8	21 9 14 15	1	0 1 1	0 1 1	1.71E-03
MKRN1	LARP1	16	19 20 17 7	18 15 25 12	1	1 1 0	0 1 1	1.71E-03
MKRN1	G3BP2	13	12 14 20 8	18 10 21 9	2	0 1 3	0 3 0	3.07E-03
MKRN1	hnRNP AB	6	6 6 12 8	5 7 9 7	2	1 4 3	0 3 2	3.91E-03
MKRN1	ATAD3A	8	11 12 4 4	11 13 8 7	0	0 0 0	0 0 0	4.64E-03
MKRN1	NUFIP2	10	13 13 8 3	17 9 13 7	0	0 0 0	0 0 0	6.40E-03
MKRN1	IGF2BP3	8	13 5 14 6	9 4 13 9	0	0 0 0	0 0 0	6.40E-03
MKRN1	MKRN1	11	27 12 14 11	10 9 23 14	0	0 0 0	0 0 0	6.44E-03
MKRN1	DHX9	10	15 12 6 4	11 5 14 13	2	0 1 0	0 2 0	6.44E-03
MKRN1	hnRNP D	4	7 6 6 6	5 1 4 4	2	0 2 2	0 1 1	6.75E-03
MKRN1	G3BP1	19	41 30 27 18	52 15 24 16	2	0 2 0	0 0 0	8.30E-03
MKRN1	LIN28A	3	4 4 4 2	1 2 5 2	1	0 1 0	0 0 0	8.30E-03
MKRN1	PABPN1	3	3 2 4 3	1 4 6 4	0	0 0 0	0 0 0	8.30E-03
MKRN1	ATXN2L	12	18 10 15 4	22 8 18 9	0	0 0 0	0 0 0	8.30E-03
MKRN1	MATR3	6	6 5 7 7	6 2 12 4	1	0 0 0	1 1 0	9.18E-03
MKRN1	UPF1	17	14 9 34 11	26 15 25 10	0	0 0 0	0 0 0	1.14E-02
MKRN1	hnRNP L	9	7 5 12 11	7 5 18 8	2	0 2 1	0 0 2	1.33E-02
MKRN1	EIF4G1	23	28 22 32 13	15 6 45 19	0	0 0 0	0 0 0	1.64E-02
MKRN1	USP10	8	11 11 8 3	14 4 14 3	0	0 0 0	0 0 0	1.64E-02
MKRN1	DDX1	5	6 3 4 2	10 3 9 5	0	0 0 0	0 0 0	1.64E-02
MKRN1	LARP4	7	9 6 16 3	7 3 10 6	0	0 0 0	0 0 0	1.79E-02
MKRN1	LARP4b	2	0 1 1 2	1 1 1 2	0	0 0 0	0 0 0	1.79E-02
MKRN1	2700060E02Rik	3	2 3 2 1	6 3 3 1	0	0 0 0	0 0 0	2.35E-02
MKRN1	FIP1L1	3	4 6 1 2	1 2 3 3	0	0 0 0	0 0 0	2.35E-02
MKRN1	ILF2	11	3 3 3 2	1 1 6 2	1	0 0 0	0 0 0	2.35E-02
MKRN1	P11260	6	6 11 3 2	6 3 3 1	0	0 0 0	0 0 0	2.35E-02
MKRN1	BAT2L2	11	18 8 11 3	19 2 17 7	0	0 0 0	0 0 0	2.68E-02
MKRN1	HADHA	9	8 10 13 3	4 5 17 4	0	0 0 0	0 0 0	2.68E-02
MKRN1	CPSF6	2	1 0 2 1	1 0 2 1	0	0 0 0	0 0 1	2.68E-02
MKRN1	FAM98A	2	1 1 1 1	2 1 2 2	0	0 0 0	0 0 0	2.68E-02
MKRN1	AGO2	2	1 1 5 3	3 1 3 1	0	0 0 0	0 0 0	3.16E-02

Table 1. (continued)

Bait	FLAG:MKRN1-associated proteins	FLAG:MKRN1 IP			FLAG:Ctrl IP			Adjusted <i>P</i> -value
		Mean UPEP	Spectral counts		Mean UPEP	Spectral counts		
			–MG132	+MG132		–MG132	+MG132	
MKRN1	DDX3X	10	9 0 13 9	11 3 14 11	5	0 6 0	0 0 3	3.47E-02
MKRN1	MOV10	12	10 10 22 4	7 7 25 5	0	0 0 0	0 0 0	4.03E-02
MKRN1	CASC3	3	2 4 5 0	3 4 2 0	0	0 0 0	0 0 0	4.46E-02
MKRN1	FXR1	8	9 6 10 2	13 1 16 5	2	0 1 0	0 3 0	4.71E-02
MKRN1	SRRT	2	1 1 2 2	0 0 2 2	0	0 0 0	0 0 0	4.72E-02

FLAG:MKRN1-associated proteins (UniProt/SwissProt gene names) identified from replicate AP-MS experiments performed in the presence or absence of the proteasome inhibitor, MG132. Spectral counts are provided for each of the biological replicates detected from the FLAG:MKRN1 and FLAG:Ctrl purifications. FLAG:MKRN1-associated proteins are designated as those with an adjusted *P*-value < 0.05. Adjusted *P*-values were calculated using the Benjamini–Hochberg method. Mean unique peptide counts (UPEP) for each purified protein are listed. For the complete unfiltered data, see Table EV1.

FLAG:MKRN1 RIP data set to those transcripts expressed at signals detected above background in undifferentiated ESC populations. The resultant filtered FLAG:MKRN1 RIP data set data set yielded 1,870 transcripts, which we refer to as the MKRN1–mRNA network. Of the 1,870 transcripts, 1,736 (92.8%) were from the middle bin and are considered low-abundance mRNAs, while the remaining 134 (7.2%) were from the high bin and are considered high-abundance messages. Thus, the MKRN1–mRNA network is primarily populated with transcripts that are detected in low abundance in mESC populations and principally devoid of high-abundance messages (Fig 4A).

To examine whether the prevalence of low-abundance mRNAs in the MKRN1–mRNA network was due to MKRN1-mediated degradation of its target mRNAs, microarray expression data from MKRN1-depleted ESC populations were overlaid with the MKRN1 RIP data set to determine the extent of overlap between the two data sets with the expectation that MKRN1-associated mRNAs that are also differentially expressed upon the temporal repression of MKRN1 expression potentially represent transcripts whose steady-state abundance is sensitive to MKRN1 availability. To capture the early response dynamics of the ESC transcriptome downstream of MKRN1 suppression, MKRN1 was knocked down via transient transfection of short hairpin RNA (shRNA) in undifferentiated ESC populations resulting in more than twofold reduction in *Mkrm1* mRNA expression compared to shGFP-transfected control ESCs (Fig EV4A). Notably, shMKRN1-transfected ESC populations remained undifferentiated six days post-transfection as indicated by sustained *Oct4* and *Nanog* mRNA expression and positive alkaline phosphatase staining (Fig EV4A and B), thereby permitting direct comparison of the microarray expression and RIP-chip data sets, which were both derived from undifferentiated ESC populations.

Global changes in gene expression in MKRN1-depleted ESC populations were examined using Affymetrix Mouse Gene 1.0 ST microarrays. From this transcriptomic analysis, 411 unique transcripts were identified as differentially expressed via pairwise statistical comparison (FDR < 0.05) between microarray data from shGFP- and shMKRN1-transfected ESC populations (Table EV4). Of these differentially expressed transcripts, only 45 overlapped with the MKRN1 RIP data set (Fig 4B). This degree of overlap was not considered statistically significant ( $P = 0.226$ ; two-tailed Fisher's exact test), suggesting that at the global level, MKRN1 does not regulate the steady-state abundance of its associated mRNAs.

Nevertheless, our integrative network analysis revealed a cluster of MKRN1-associated transcripts whose abundance tends to be dependent on MKRN1 availability. We infer that these transcripts represent a MKRN1-dependent gene regulatory module embedded within the MKRN1–mRNA network (Fig 4C).

To verify that the depletion of MKRN1 affects the abundance of mRNAs found within this module, eight representative transcripts from the module were selected for further validation in a stable MKRN1 knockdown ESC clone which exhibited sustained and robust ablation of MKRN1 (Fig EV1B). The steady-state abundance of the eight representative MKRN1-associated mRNAs was similarly affected in stable MKRN1 knockdown ESC populations relative to a stable shGFP control clone, confirming the transcriptomic analysis from transient MKRN1 knockdown ESC populations (Fig 4D). Additionally, the enrichment of five predicted FLAG:MKRN1-associated mRNAs were validated using RIP-qPCR. Four of the five predicted FLAG:MKRN1-associated mRNAs exhibited mean fold enrichment values above threshold (Fig 4E), collectively suggesting that this cluster of transcripts represents a MKRN1-mediated posttranscriptional gene regulatory module in ESCs.

Therefore, our integrative network analysis suggests that MKRN1 modulates the steady-state abundance of a small subset of its associated mRNAs in ESCs; however, this mode of regulation is insufficient to explain the prevalence of low-abundance messages within the MKRN1–mRNA network and thus points to alternate posttranscriptional gene regulatory mechanisms for MKRN1 in mRNA metabolism.

#### Functional classification of the MKRN1–mRNA network reveals that MKRN1 targets mRNAs that localize to the ER

To gain further insight into alternate roles for MKRN1 in mRNA metabolism, we performed gene-annotation enrichment analysis in DAVID to cluster the MKRN1–mRNA network into functionally related gene sets. Low-abundance transcripts (middle bin) and high-abundance transcripts (high bin) were queried independently to generate separate enrichment maps [46]. The middle and high bin yielded distinct enrichment maps (Fig 5 and Table 2). Gene-annotation enrichment analysis of the low-abundance transcripts identified terms indicative of diverse biological processes including signal transduction ( $P = 1.2E-05$ ), cell differentiation ( $P = 9.1E-06$ ), and cell death ( $P = 2.7E-04$ ) (Table 2). In contrast, transcripts in the

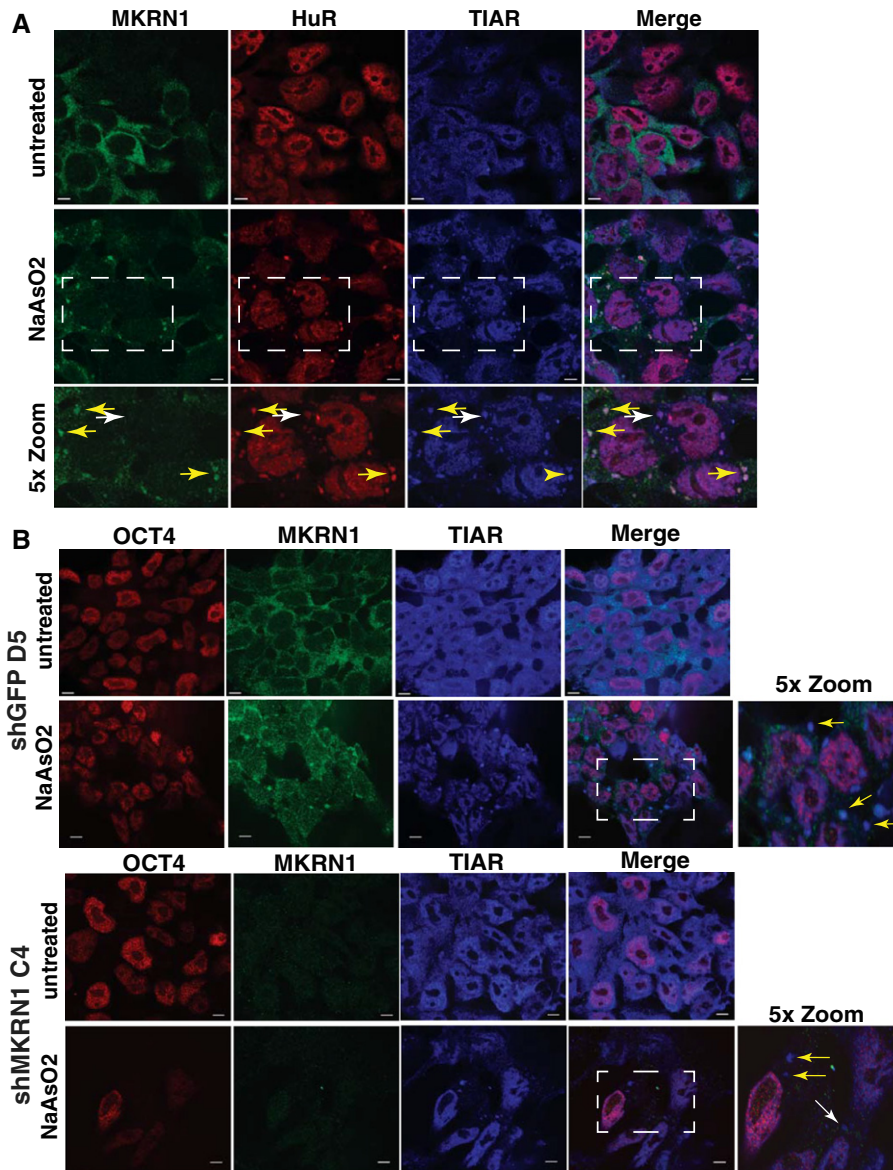


**Figure 3. MKRN1 is mobilized to SGs, but is not required for SG formation.**

- A Recruitment of endogenous MKRN1 in SGs in R1 ESCs stressed for 1 h with 1 mM NaAsO<sub>2</sub> (+NaAsO<sub>2</sub>). SG formation was monitored with HuR and TIAR immunostaining. Yellow arrows indicate MKRN1/HuR/TIAR-positive SGs; white arrows indicate SGs devoid of MKRN1. Enlargements of boxed regions are indicated as 5× zoom.
- B MKRN1 is not absolutely required for SG assembly in undifferentiated ESCs. MKRN1 knockdown and shGFP control ESC clones were stressed as in (A). Yellow arrows indicate TIAR-positive SGs in OCT4<sup>+</sup> ESCs; white arrows indicate TIAR-positive SGs in OCT4<sup>-</sup> ESCs. Scale bars: 10 μm. Enlargements of boxed regions are indicated as 5× zoom.

high bin were not enriched for terms specific to any biological processes; yet, both the middle and high bins were strongly enriched for terms related to cellular components, specifically transcripts encoding secretory proteins ( $P = 2.0E-09$ ), integral membrane proteins ( $P = 3.2E-04$ ), signal-peptide-containing proteins ( $P = 9.7E-07$ ), and intracellular membrane-bound proteins ( $P = 1.3E-05$ ) including 14 ER-resident proteins, suggesting that MKRN1-containing mRNPs preferentially harbor mRNAs destined for translation at the ER (Fig 5 and Table 2).

Most mRNAs encoding transmembrane and secreted proteins are anchored on the ER by the signal recognition particle pathway to

allow co-translational translocation of the signal peptide into the ER. Yet, mRNAs encoding secreted, integral membrane, and ER-resident proteins (mSMERPs) also localize to the ER independently of translation in a process thought to involve RBP-mediated mRNP transport [47]. Given the strong enrichment of mSMERPs in the MKRN1–mRNA network, we tested whether the depletion of MKRN1 alters localization of its target mSMERPs to the ER. Hence, the distribution of MKRN1 target mSMERPs in the ER-enriched subcellular fraction relative to the soluble (cytosolic) fraction was quantified from MKRN1 knockdown and control ESC lysates by qPCR. To decouple MKRN1-mediated translocation of mRNAs to the

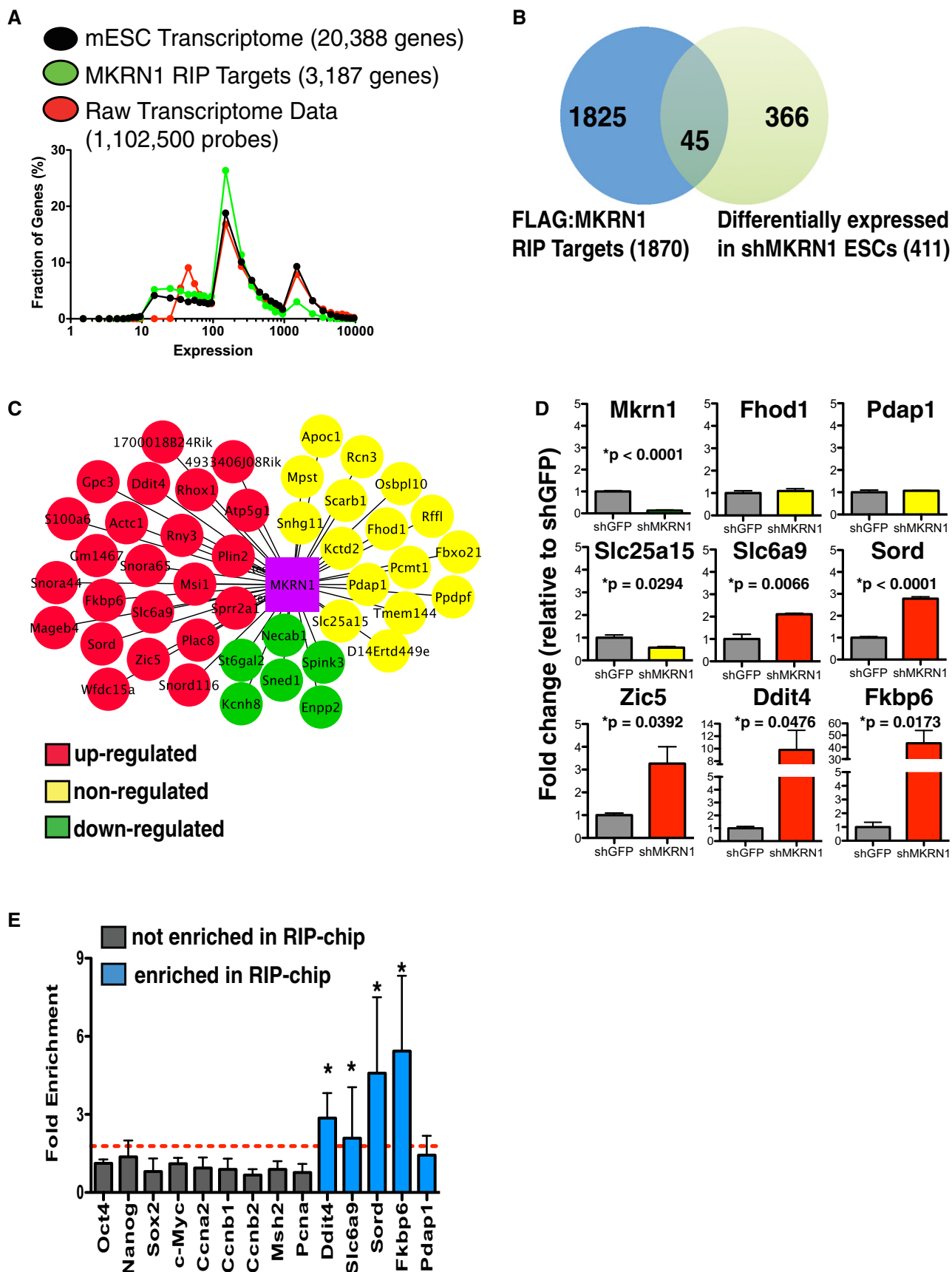


Figure 4.

**Figure 4. Integrative genomic analysis of the MKRN1–mRNA network.**

- A Histograms comparing the distribution of mRNA abundance for transcripts in the MKRN1–mRNA network with > 20,000 transcripts representing the ESC transcriptome. Further details are provided in Materials and Methods.
- B Venn diagram shows the overlap of transcripts in the MKRN1–mRNA network with the 411 differentially expressed transcripts identified from the transient MKRN1 knockdown microarray data set.
- C Network diagram of the 45 transcripts identified in (B). Node color corresponds to the extent each transcript was differentially expressed in the transient MKRN1 knockdown microarray data set.
- D qPCR data from stable MKRN1 knockdown ESCs validate the microarray data set. Colored bars represent the fold change in abundance of eight FLAG:MKRN1-associated mRNAs from (C) in the stable shMKRN1 ESC clone C4 relative to a stable shGFP control clone (gray bars). Bar color scheme is the same as (C) and corresponds to the extent the mRNA was differentially expressed in the transient MKRN1 knockdown microarray data set. Data are means  $\pm$  SEM from three biological replicate experiments ( $P$ -values are indicated, two-tailed  $t$ -test).
- E RIP-qPCR experiments were performed in triplicate to corroborate the findings from the RIP-chip analysis. RIP-qPCR experiments confirmed that the predicted FLAG:MKRN1 RIP targets (blue bars) were enriched in FLAG:MKRN1 RIPs versus a subset of transcripts not detected as enriched from the RIP-chip analysis (gray bars) ( $P < 0.001$ ; Mann Whitney  $U$ -test). Asterisks denote the four of the five predicted FLAG:MKRN1 RIP targets with mean fold enrichment values above the specified threshold (red line) calculated as two standard deviations (SD) from the mean fold enrichment of the negative control group (gray bars). Data are means  $\pm$  SD from three biological replicate experiments.

ER from ribosome-dependent anchorage of mRNAs at the ER membrane, we also compared the relative abundance of mSMERPs in each subcellular fraction from ESC lysates pre-treated with EDTA prior to ultracentrifugation to elicit ribosome disassembly. Immunoblot analysis confirmed that the ER luminal protein marker calnexin was detected in ER-enriched fractions, but not soluble (cytosolic) fractions, and that EDTA treatment effectively dissociated mRNPs from ER-enriched lysates (Fig EV4C).

The relative ER-to-cytosolic distribution of seven MKRN1 target mSMERPs (*Cnpy3*, *Prkcsh*, *Glt25d1*, *Slc6a9*, *Fzd2*, *Gpc3*, and *Txndc5*) and four non-MKRN1 target mRNAs (*Oct4* [soluble protein; negative control], and *E-cadherin*, *Lamp1*, and *Epcam* [secreted proteins; positive controls]) was assessed by qPCR. As expected, the representative mSMERPs including *E-cadherin*, *Lamp1*, and *Epcam* were highly enriched in the ER-enriched fraction relative to the soluble fraction, and this enrichment was attenuated in EDTA-treated lysates (Fig EV4D), signifying the release of mSMERPs from membrane-bound ribosomes. Depletion of MKRN1 had little effect on the ER-to-cytosol distribution of the seven MKRN1 target mSMERPs, as the mRNA distribution was comparable in both MKRN1 knockdown and control lysates, irrespective of EDTA treatment (Fig EV4E).

Consistent with the finding that MKRN1 is dispensable for the translocation of mRNAs to the ER, immunoblot analysis also indicated that MKRN1 is most abundant in the soluble cytosolic fraction, and comparatively only modestly present in the ER-enriched fraction (Fig EV4C). These data verify that MKRN1 associates with mRNAs that are ultimately localized to the ER, and suggest that the principal

**Table 2. Functional annotation categories for enriched functional related gene sets in the MKRN1–mRNA network.**

	Number of transcripts in gene set	$P$ -value	Adjusted $P$ -value
Functionally related gene sets			
Low-abundance transcripts			
Secreted	182	2.0E-09	5.0E-07
Collagen	26	1.3E-08	2.1E-06
Signal peptide	336	9.7E-07	3.2E-03
Extracellular matrix	53	1.1E-06	1.6E-04
Transcription factor activity	98	6.4E-06	2.1E-03
Cell differentiation	184	9.1E-06	7.9E-04
Regulation of signal transduction	87	1.2E-05	3.4E-03
Transport/localization	246	1.3E-05	3.2E-03
Regulation of catalytic activity	65	2.5E-05	4.7E-03
Regulation of cell death (apoptosis)	71	2.7E-04	3.8E-02
Plasma membrane	291	3.2E-04	2.3E-03
Neuron differentiation	53	4.8E-04	5.2E-03
Functionally related gene sets			
High-abundance transcripts			
Acetylation	35	4.8E-06	8.8E-04
Intracellular membrane-bound	72	1.3E-05	6.2E-04
Endoplasmic reticulum	14	4.2E-03	6.9E-02

List of functionally relevant gene lists in each of the two subgroups of the MKRN1–mRNA network.  $P$ -values represent the EASE score (modified Fisher's exact  $P$ -value for gene-enrichment analysis) calculated in DAVID. Adjusted  $P$ -values were calculated using the Benjamini–Hochberg method (FDR < 0.1). FLAG:MKRN1-associated mRNAs comprising each listed term are provided in Table EV5.

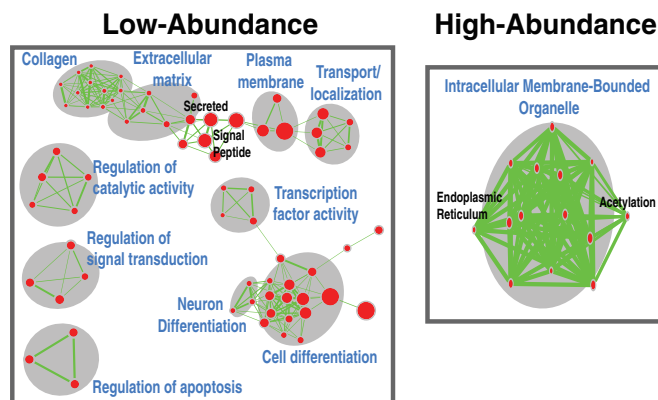


**Figure 5. The MKRN1–mRNA network is enriched for transcripts encoding functionally related proteins.**

Enrichment map representation of enriched cellular and biological processes for low- and high-abundance mRNAs in the MKRN1–mRNA network ( $P < 0.005$ ; FDR < 0.1). Nodes and edges are represented as described in Material and Methods. Additional information related to the labeled nodes is provided in Table 2.

mode for their enrichment in ER-enriched fractions is via associations with membrane-bound ribosomes.

### Contribution of MKRN1 in early apoptotic signaling during cellular stress

Motivated by (i) our findings that MKRN1 is a novel SG-resident protein, (ii) the MKRN1–mRNA network is enriched for mRNAs encoding apoptosis-related proteins, and (iii) recent publications describing full-length MKRN1 as a pro- and/or anti-apoptotic protein downstream from various stress responses in transformed cell lines [23,24], we asked whether MKRN1 modulates the apoptotic fate of ESCs downstream from stress responses that either do or do not induce SG formation. To monitor the extent of apoptotic pathway activation from stressed MKRN1 overexpression and knockdown ESC clones, immunoblot analysis was performed on lysates collected 4 h after NaAsO<sub>2</sub>-induced oxidative stress (SG-inducing stress) and following 6 h of sustained adriamycin (ADR)-induced genotoxic stress (non-SG-inducing stress).

Exposure of ESCs to NaAsO<sub>2</sub> initiates a p53-independent oxidative stress response that is marked by the activation of the intrinsic apoptosis pathway, and concomitant silencing of the self-renewal GRN [48]. Accordingly, exposure of MKRN1 transgenic ESC clones to NaAsO<sub>2</sub> led to a dramatic decrease in OCT4 protein abundance as well as visible increases in cleaved caspase-3 and cleaved PARP levels, but not the genotoxic stress marker p53 (Fig 6A and B), indicating that an oxidative stress response was activated in all ESC clones tested. Manipulation of MKRN1 expression had a modest, yet statistically significant, effect on the abundance of early apoptotic markers in NaAsO<sub>2</sub>-stressed ESC populations (Fig 6A and B). Notably, while MKRN1 overexpression had a negligible effect on PARP cleavage (a marker of apoptogenic signaling) following NaAsO<sub>2</sub> exposure (Fig 6A), knockdown of MKRN1 in NaAsO<sub>2</sub>-stressed ESC populations was associated with enhanced PARP cleavage (Fig 6B). Despite reports of the contrary in other cell types [23,24], inhibition of MKRN1 did not result in spontaneous ESC death or the upregulation of p53 in unstressed conditions (Fig 6B), suggesting that MKRN1 selectively functions to restrict the activation of apoptotic pathways in ESCs downstream from an SG-mediated stress response.

Some SG-resident proteins mediate distinct cellular responses to stress that are dependent on the type of stress encountered [49–51]. Given that MKRN1 reportedly functions as a pro-apoptotic protein in U2OS cells in response to ADR-induced genotoxic stress [24], we tested whether MKRN1 promotes apoptosis in ESCs downstream of the ADR-induced genotoxic stress response that is known not to induce SG formation [52]. ADR has previously been shown to induce genotoxic stress in ESC populations [53–55]; however, to confirm that ADR treatment does not cause SG formation, the subcellular localization of MKRN1 and the SG marker, HuR, were examined in ADR-treated ESC populations. As expected, neither MKRN1 nor HuR was found coalesced into cytoplasmic foci in ADR-treated ESCs (Fig EV5A and B), confirming that following ADR-induced genotoxic stress, MKRN1 remains in the cytoplasm.

To assess whether manipulated MKRN1 expression altered the susceptibility of ESCs to initiate ADR-induced apoptosis, apoptosis marker abundance in ADR-treated MKRN1 transgenic ESC clones was compared to their respective control clones following 6 h of sustained ADR exposure. In contrast to our findings from

NaAsO<sub>2</sub>-treated ESC populations, the depletion of MKRN1 was not associated with increased cleaved PARP following 6 h ADR treatment (Fig 7A), suggesting differences in MKRN1 function between the oxidative and genotoxic stress responses. Indeed, while the overexpression of MKRN1 had no discernable effect on the extent of PARP cleavage following NaAsO<sub>2</sub> exposure (Fig 6A); downstream from genotoxic stress, elevated MKRN1 expression was associated with enhanced p53 stability and heightened PARP cleavage (Fig 7B). Taken together, these data suggest that increased MKRN1 availability enhances the activation of apoptotic pathways in ESC populations undergoing genotoxic stress, whereas the suppression of MKRN1 augments apoptosis signaling in ESC populations recovering from environmental stress.

### A granular apoptotic gene regulatory module within the MKRN1–mRNA network

To gain insight into how MKRN1 could modulate apoptosis in ESCs during the genotoxic stress response via posttranscriptional regulatory interactions, we drafted a MKRN1 apoptotic gene regulatory network module that consisted of the 76 apoptosis-related transcripts embedded within our MKRN1–mRNA network. Interestingly, despite MKRN1 binding, these transcripts are not differentially expressed upon loss of MKRN1 in ESCs, suggesting alternate modes of MKRN1-mediated posttranscriptional regulation outside the control of mRNA turnover. To understand how these mRNAs are regulated in ESCs, published genomic data from unstressed and ADR-treated mESCs [10,54] were integrated with our data to yield a granular MKRN1-centered apoptotic gene regulatory module (Fig 8). From this integrative genomic analysis, two important features of this module were revealed. First, MKRN1 is associated with apoptotic transcripts that are transcriptional targets of various transcription factors, suggesting that MKRN1 may coordinate a distinct regulatory program within the ESC GRN through consolidation of messages from diverse transcriptional programs. Second, of the 76 apoptosis-related MKRN1 target transcripts, only ~20% are differentially expressed at the transcriptional level during the ESC DNA damage response [54], implicating these targets as strong candidates for MKRN1-mediated posttranscriptional regulation during genotoxic stress.

## Discussion

Considerable insight into the intricate architecture of the ESC GRN has been gained by integrating data from proteomic studies, promoter occupancy studies, dynamic transcriptomic analysis, and gain-/loss-of-function assays [9–16]; however, to date, our understanding of the ESC GRN has been centered around the maintenance of pluripotency and self-renewal. Consequently, many critical nodes of the ESC GRN have been discerned and the topology of this network is thought to be a concentric hub of positive feedback and feed-forward modules. However, to capture the complexity of ESC identity, GRN nodes that are not functionally linked to self-renewal or pluripotency should also be analyzed in depth. Using an unbiased analysis of the *Mkfn1* node, we demonstrate the utility of a multidimensional integrative genomics approach to discern the function of uncharacterized nodes in the ESC GRN.

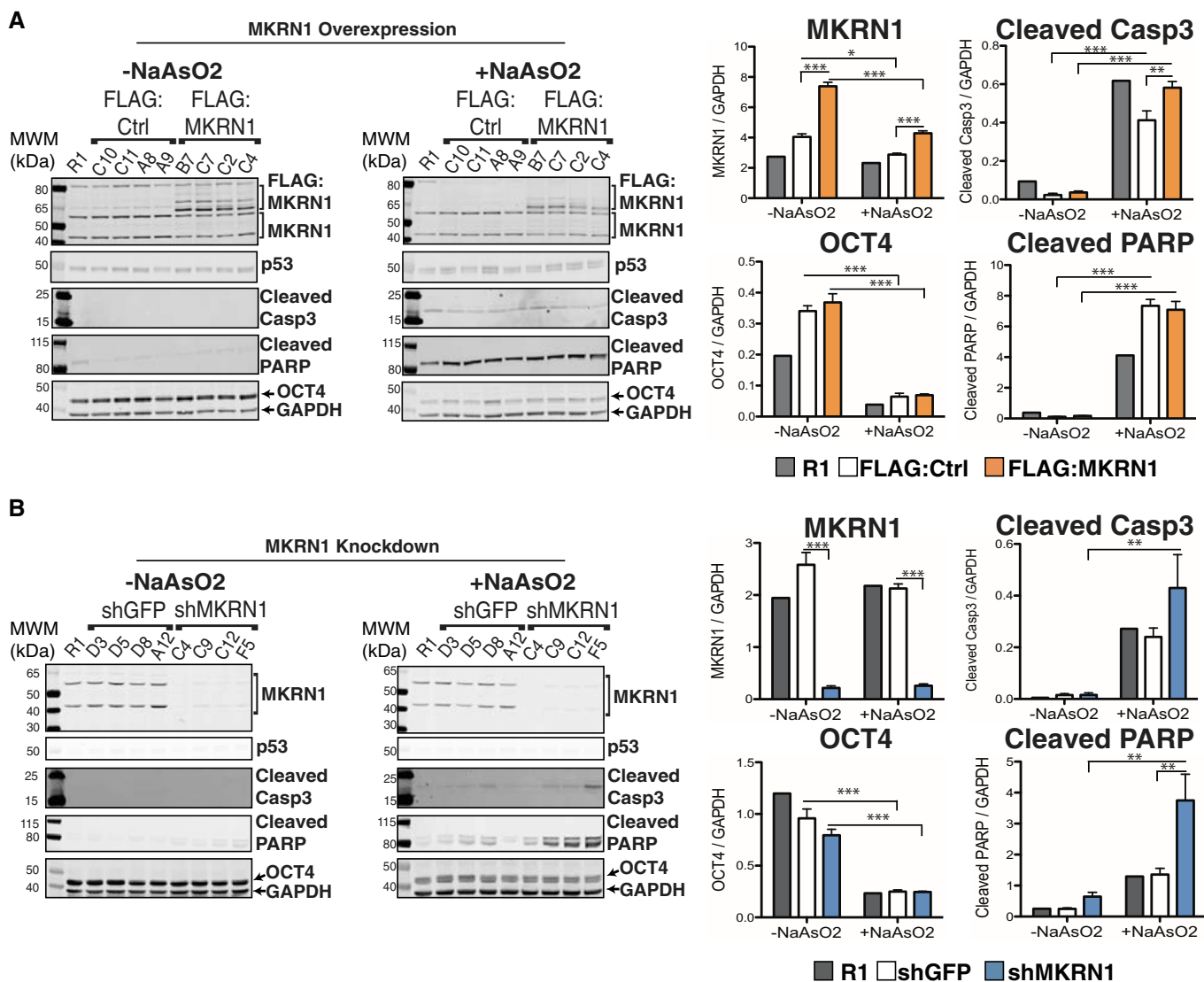


**Figure 6.** ESC populations depleted of MKRN1 exhibit increased PARP cleavage following recovery from oxidative stress.

A, B Control and MKRN1 overexpression (A) or knockdown (B) ESC clones were either untreated ( $-NaAsO_2$ ) or stressed for 30 min with 1 mM  $NaAsO_2$  and allowed to recover for 4 h ( $+NaAsO_2$ ) prior to lysis. Total p53 served as an indicator of genotoxic stress. MKRN1, OCT4, cleaved caspase-3, and cleaved PARP are quantified relative to GAPDH and are presented to the right of the respective immunoblots. Data are means of four independent clones in each group from two biological replicate experiments  $\pm$  SEM. Statistically significant differences in mean protein abundance between populations are indicated by \* $P < 0.05$ , \*\* $P < 0.01$ , or \*\*\* $P < 0.001$  (two-way ANOVA).

Source data are available online for this figure.

Here, we report an additional molecular function for the E3 ubiquitin ligase protein MKRN1 as a potential RBP and an mRNP component that is localized to SGs in response to environmental stress. Principal evidence for such function is provided from our unbiased AP-MS analysis, which repeatedly detected FLAG:MKRN1 associated with 35 annotated RBPs (Table 1). Among these RBPs, we found that full-length MKRN1 interacts with established mRNA-binding proteins including PABPC1, PABPC4, LITD1, and YBX1 independently of RNA (Fig 2C). Consistent with these data, Miroci *et al* (2012) reported a direct interaction between PABPC1 and recombinant MKRN1-short isoform in HEK 293 cells [26]. The MKRN1-short isoform lacks the  $C_3HC_4$  RING domain, which Miroci

*et al* (2012) reasoned imparts ribonucleoprotein function to the MKRN1-short isoform rather than E3 ubiquitin ligase activity. Here, we show that full-length FLAG:MKRN1 protein, which contains the  $C_3HC_4$  RING domain, interacts with several endogenous mRNA-binding proteins and RNA (Fig 2E), indicating that the presence of the  $C_3HC_4$  RING domain does not preclude MKRN1 association in mRNPs. Indeed, several other RING domain-containing proteins including Roquin [56,57], MEX-3 [58], and CNOT4 [59] also form mRNP complexes implicating this class of E3 ubiquitin ligase proteins as a novel class of gene regulatory proteins [27].

In further support that full-length MKRN1 harbors RNA-binding capacity, our CLIP experiments show that IP of cross-linked (but not

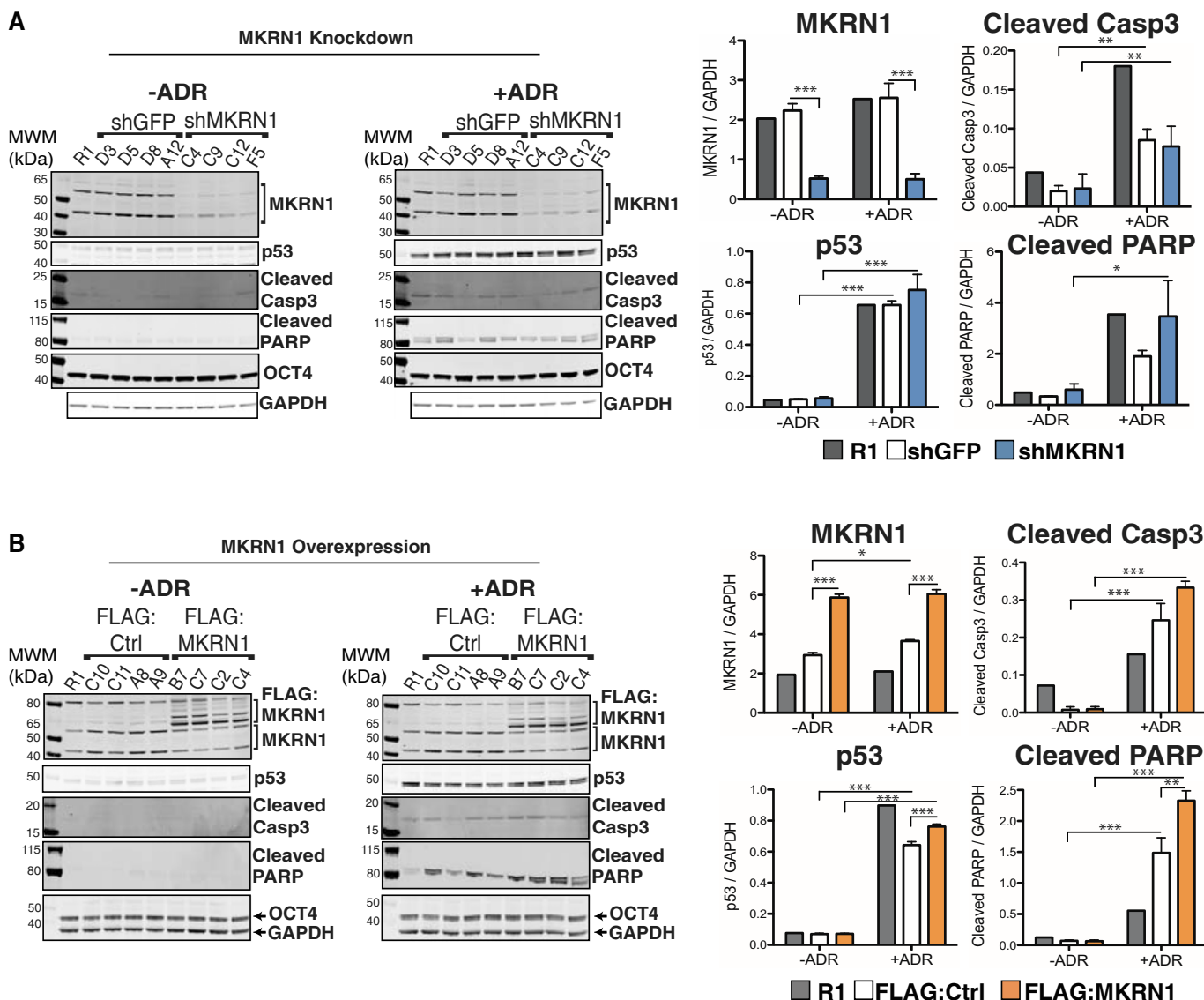


**Figure 7. MKRN1 overexpression ESC populations exhibit increased expression of early apoptotic markers downstream of ADR-induced genotoxic stress.**

A, B Control and MKRN1 knockdown (A) or overexpression (B) ESC clones were either untreated (–ADR) or stressed with 0.5  $\mu$ M ADR for 6 h (+ADR) prior to lysis. MKRN1, p53, cleaved caspase-3, and cleaved PARP are quantified relative to GAPDH and are presented to the right of the respective immunoblots. Data are means of four independent clones in each group from two biological replicate experiments  $\pm$  SEM. Statistically significant differences in mean protein abundance between populations are indicated by \* $P < 0.05$ , \*\* $P < 0.01$ , or \*\*\* $P < 0.001$  (two-way ANOVA).

Source data are available online for this figure.

uncross-linked) FLAG:MKRN1 co-purifies with RNA, and, the size of the purified protein–RNA complexes corresponds to the size of supershifted MKRN1 proteins that are cross-linked to RNA (Fig 2F). Importantly, the molecular weight of immunoprecipitated FLAG:MKRN1–RNA complexes demonstrated sensitivity to RNase treatment, thereby confirming that purified FLAG:MKRN1 complexes contain RNA. Finally, the presence of MKRN1’s four C<sub>3</sub>H zinc finger RNA-binding domains underlines our contention that MKRN1 is a genuine RNA-binding protein.

While MKRN1 has previously been shown to stimulate translation when tethered to a reporter transcript as a  $\lambda$ N<sub>22</sub>-fusion protein [26], here we provide evidence to suggest that MKRN1 is capable of mRNA

regulation without the requirement of additional RBPs to facilitate mRNA binding. Consistent with this, unbiased oligo(dt) capture experiments identified MKRN1 as one of the 860 proteins that was pulled down with UV-cross-linked polyadenylated mRNA from HeLa cell lysates [60]. Interestingly, however, MKRN1 was not identified as one of the 555 proteins that directly binds poly(A)-mRNA in an analogous oligo(dt) capture experiment performed from mESC populations [61]. The discrepancy in findings between the two studies may be explained by the dependency of the oligo(dt) capture method on mass spectrometry analysis to identify all enriched proteins from a complex sample, which increases susceptibility for false negatives. Moreover, oligo(dt) capture is biased toward the most abundant transcripts and

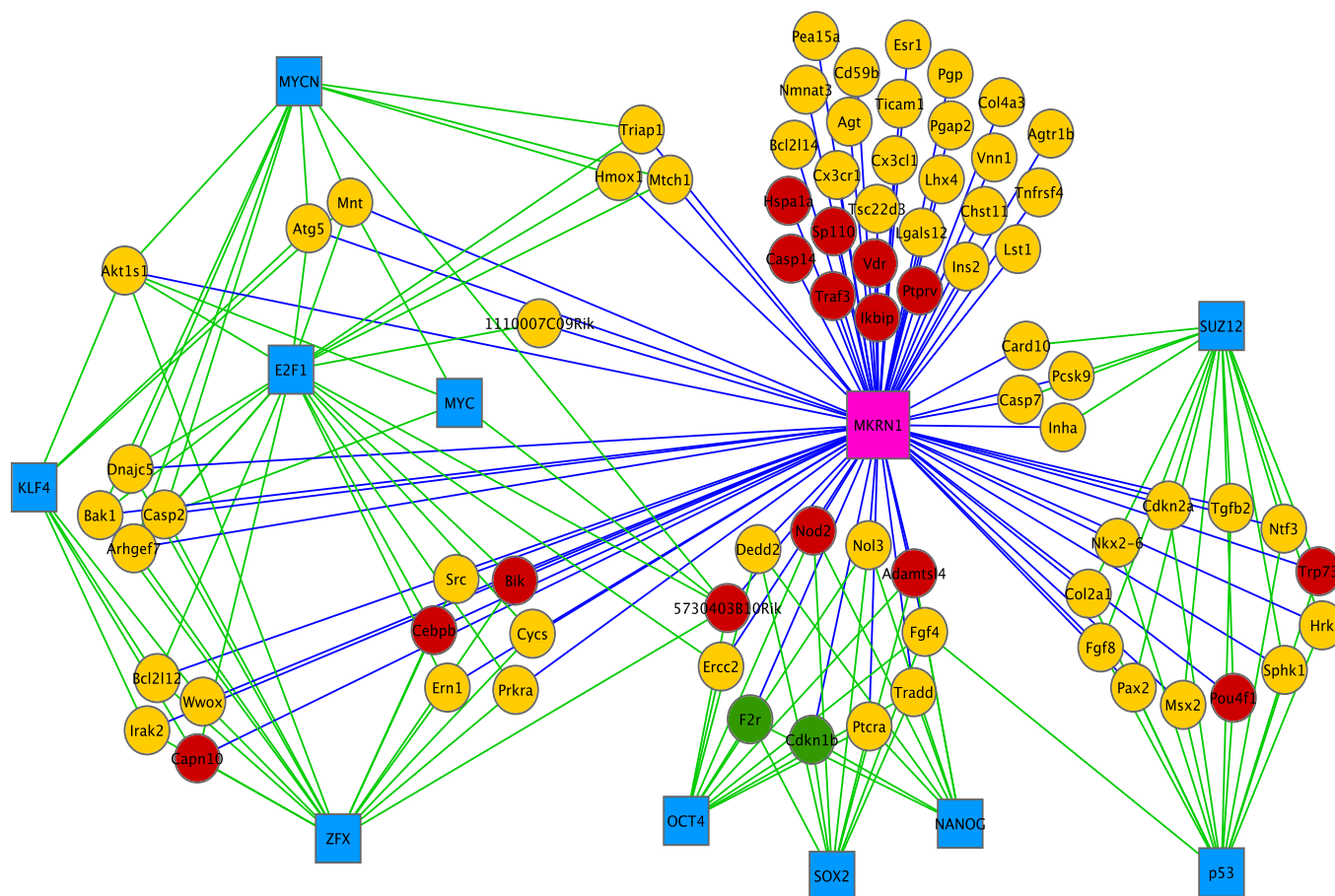


**Figure 8. A granular apoptotic gene regulatory module embedded in the MKRN1-mRNA network.**

Seventy-six apoptosis-related transcripts identified in the MKRN1-mRNA network are shown as circular nodes. Blue edges denote MKRN1-mRNA associations. Green edges specify occupancy of ESC-associated transcription factors (blue squares) at the respective gene's promoter based on published data [10,54]. Circular node color indicates whether the transcript was upregulated (red), downregulated (green), or not differentially expressed (yellow) in ADR-treated R1 ESCs [54].

may not capture RBPs bound to less abundant mRNAs. Thus, while we have been unable to provide definitive evidence of direct binding of RNA by MKRN1, our targeted CLIP experiments suggest that MKRN1 exhibits RNA-binding capacity in ESC populations.

Using RIP-chip, we identified 1,870 unique transcripts selectively associated with FLAG:MKRN1 in ESC populations. The MKRN1-mRNA network was more extensive than initially anticipated, but comparable in breadth to other annotated protein-mRNA networks [62–69]. Although the exact requirements for mRNA recognition remain to be defined, we find that MKRN1 preferentially occupies low-abundance mRNAs (Fig 4A); yet, MKRN1 is not required for the stability of most of its associated mRNAs (Fig 4B). This observation is consistent with the absence of deadenylases, decapping factors, or components of the exosome (a multimeric complex involved in 3′–5′ degradation of labile mRNAs) in the MKRN1 AP-MS data set. Moreover, although MKRN1 is present in SGs (Fig 3A), MKRN1 is not found in processing bodies (unpublished observations), which are cytoplasmic sites of active mRNA decapping and decay [70]. In sum, our data suggest that as a component of mRNPs, MKRN1 does not principally regulate mRNA turnover and instead points to alternate roles for MKRN1 in mRNA metabolism. Consistent with this assertion, it has been shown that MKRN1 does not

affect the stability of a reporter transcript to which it was tethered, but rather regulates its translation [26].

To date, the interpretation of MKRN1 activity in mammalian systems has been dominated by reports of MKRN1-mediated E3 ubiquitin ligase activity toward various tumor suppressor proteins including p21, p53, and p19<sup>ARF</sup> [20,23,24]. While these studies provide compelling evidence that MKRN1 regulates tumor cell survival and proliferation, it is important to note that several of the reported MKRN1 substrate proteins, notably p21 and p19<sup>ARF</sup>, are not expressed in undifferentiated mESCs [71,72], which may explain why these proteins were not identified in our AP-MS analyses. Furthermore, contrary to previous reports, the depletion of MKRN1 in unstressed ESC populations did not result in apoptosis, enhanced p53 protein stability, or cell cycle arrest (Figs 6 and 7 and unpublished observations). Taken together, the discrepancies between our findings and those of Song and colleagues [20,23,24] imply that the function of MKRN1 is context dependent and influenced by both the cell type and the cellular environment, consistent with our finding that MKRN1 positively and negatively influences early apoptotic signaling events dependent on the type of stress response evoked (Figs 6 and 7).

Motivated by reports of a proapoptotic role for MKRN1 following DNA damage in the human osteosarcoma U2OS cell line [24], here

we tested whether the manipulation of MKRN1 expression affects the apoptotic fate of ESCs undergoing ADR-induced genotoxic stress. Based on the findings of Lee *et al* (2009), we expected MKRN1-depleted ESCs to harbor a heightened tolerance for genotoxic stress, and conversely gain of MKRN1 function to sensitize ESCs to ADR-induced apoptosis. Overall, manipulation of MKRN1 expression did not dramatically affect apoptotic events in ADR-treated ESC populations (Fig 7 and unpublished observations); however, similar to findings from MKRN1 overexpression experiments in U2OS cells, gain of MKRN1 function in ESC populations responding to genotoxic stress was associated with modest but significant increases in early apoptotic signaling markers relative to stressed control clones (Fig 7B). In contrast, the depletion of MKRN1 did not render ESC populations more resistant to ADR-induced apoptosis (Fig 7A), suggesting fundamental differences in MKRN1 function in ESCs and other cell types.

We reason that the discrepancies in cell death phenotype between transgenic MKRN1 ESC and U2OS cell populations following ADR exposure can be explained, in part, by the mechanistic differences in the DNA damage response between mESCs and differentiated cells [53,73,74]. Specifically, while somatic cells rely on p21 function for cell cycle arrest at the G<sub>1</sub> checkpoint to enable DNA damage repair (and hence survival), p21 protein expression is silenced in mESCs and therefore does not mitigate apoptosis during genotoxic stress [71,74]. In U2OS cells, MKRN1 reportedly targets p21 for ubiquitin-mediated proteolysis, thus eliminating an anti-apoptotic barrier, which in turn facilitates apoptosis initiation following DNA damage [24]. Therefore, the fact that p21 is non-functional in wild-type ESCs is consistent with our findings that the manipulation of MKRN1 expression did not yield the same dramatic apoptotic effects in ESCs. Rather, increased MKRN1 availability in ESC populations yielded a modest but significant enhancement of apoptosis signaling downstream from genotoxic stress (Fig 7B), implying a distinct mechanism for MKRN1 function during the ESC DNA damage response.

From our systems-guided analysis of MKRN1 function in ESCs, we hypothesize that MKRN1 potentiates apoptogenic signaling during the genotoxic stress response via its function within mRNPs. We report that under basal conditions, MKRN1 associates with established translational regulators, such as HuR, YBX1, and IGF2BP1 (Table 1), as well as several apoptosis-related transcripts (Fig 8). Taken together, we speculate that MKRN1 may augment the initiation of apoptotic signaling events in response to DNA damage through the translational control of an apoptotic gene regulatory program. Such posttranscriptional gene regulatory mechanisms have been described for other RBPs during the genotoxic stress response. For example, HuR mediates lymphocyte survival downstream from genotoxic stress via upregulation of anti-apoptotic proteins due to increased translation of anti-apoptotic HuR targets without significantly changing mRNA abundance [51].

In support of a comparable role for MKRN1 in activity-dependent translational control, Mohr *et al* (2012) demonstrate that in primary neural cells, MKRN1 resides in light weight ribonucleoprotein complexes devoid of large (28S) ribosomal subunits, which are indicative of translationally silent mRNPs. Yet, when tethered to a reporter mRNA, MKRN1 stimulates translation of a luciferase transcript [26], suggesting that under the appropriate conditions, MKRN1 facilitates translational initiation. These mechanistic data complement our systems-level analyses as it supports a model where under

basal conditions MKRN1 may retain its cognate mRNAs in a translationally repressed state that remain poised for translation initiation in response to certain cellular triggers, such as genotoxic stress. Future studies are required to elucidate the dynamics of the MKRN1–mRNA network in ESCs during the genotoxic stress response.

In summary, our work demonstrates the utility of an unbiased systems-guided strategy for unraveling novel functions for uncharacterized proteins in a particular cell type of interest. Our data position MKRN1 within mRNP complexes associated with several canonical mRNA regulatory proteins, which supports a regulatory function for MKRN1 in the ESC GRN. Future studies are required to uncover the precise gene regulatory mechanism of MKRN1 in ESCs, but our analyses offer additional insight into a possible role for MKRN1 as an mRNA regulatory protein. Taken together, our work contends that in addition to its E3 ubiquitin ligase activity, MKRN1 functions within mRNP complexes, and thus, comprehensive analysis of MKRN1 function should consider its role as a posttranscriptional and/or posttranslational regulatory protein.

## Materials and Methods

### ESC culture

R1 mouse ESCs were cultured in mESC media: Dulbecco's modified Eagle's medium (DMEM; GIBCO) supplemented with 15% fetal bovine serum (FBS; NorthBio Inc), 1,000 U/ml leukemia inhibitory factor (LIF; Chemicon), 0.1 mM non-essential amino acids, 1 mM sodium pyruvate, 2 mM L-glutamine, 50 µg/ml penicillin/streptomycin (GIBCO), and 10<sup>-4</sup> M β-mercaptoethanol (Sigma-Aldrich) as previously described [16]. For monolayer differentiation, ESCs initially seeded in mESC media overnight were cultured in differentiation media consisting of either mESC media without LIF or mESC media without LIF and supplemented with 100 nM retinoic acid (Sigma-Aldrich). Media were changed daily up until the indicated duration of differentiation.

### Plasmid construction and generation of transgenic MKRN1 ESC lines

shRNA sequences targeting the MKRN1 protein-coding sequence, shMKRN1 5'-GCGAGATGTTGCTTATGCTTT-3', or GFP, shGFP 5'-CACAAACAGCCACAACGTCTAT-3' were selected from the Public TRC Portal ([www.broadinstitute.org/rnai/public/](http://www.broadinstitute.org/rnai/public/)). Oligos were cloned into the pLKO.1-puro construct (a gift from J. Moffat) downstream from the human *U6* promoter as previously described [75]. The resultant pLKO.1 shRNA constructs were linearized and electroporated into undifferentiated R1 ESCs as previously described [16] to generate puromycin-resistant stable MKRN1 knockdown (shMKRN1) and control (shGFP) ESC clones.

Two distinct approaches using integrating and non-integrating systems were employed to generate MKRN1 overexpression ESC lines constitutively expressing the 3xN-FLAG:MKRN1 transgene. To generate the pCAGGS::3xN-FLAG:MKRN1 construct for stable integration into ESCs, the 3xFLAG epitope was excised from the pCMV 3xFLAG 7.1 vector (Sigma-Aldrich) with *SacI* and *XmaI*, treated with the Klenow fragment to blunt the protruding ends, and cloned into the *SmaI* site of the pCAGGS vector. The vector was linearized by

*HindIII* and treated with Klenow fragment. *Mkrr1* protein-coding cDNA was amplified, digested with *PvuII* to generate blunt ends, and ligated into the pCAGGS::FLAG vector, immediately downstream from the FLAG epitope to yield the pCAGGS::N-FLAG:MKRN1 construct. This construct was linearized and electroporated into ESCs to generate G418-resistant pCAGGS::N-FLAG:MKRN1 ESC clones, which expressed FLAG:MKRN1 at near endogenous levels and were used for unbiased detection of FLAG:MKRN1-associated proteins and mRNA.

To achieve higher levels of MKRN1 overexpression in ESCs, the 3xN-FLAG:MKRN1 transgene was expressed from the pPyCAGIP episomal system (pMGDneo20 and pPyCAGIP episomal vectors provided by J. Ellis). The pPyCAG::N-FLAG:MKRN1 episomal construct was generated by subcloning 3xN-FLAG:MKRN1 cDNA from the pCAGGS::N-FLAG:MKRN1 construct into the *XhoI/NotI*-digested pPyCAGIP episomal vector. For episomal supertransfection, a G418-resistant R1/LT line was generated to constitutively express polyoma large T (LT) from the pMGDneo20 episome. A total of  $1.7 \times 10^5$  R1/LT ESCs per well were seeded in a 12-well gelatinized plate and, 24 h later, transfected overnight with 2  $\mu$ g of supercoiled pPyCAG::FLAG:Ctrl IP or pPyCAG::FLAG:MKRN1 constructs using Lipofectamine 2000 (Life Technologies) according to the manufacturer's protocol. Transfected cells were trypsinized, pooled, and seeded on 0.1% gelatin-coated 10-cm dishes. After 48 h, ESCs were cultured in selection media (150  $\mu$ g/ml G418 and 2  $\mu$ g/ml puromycin) until isolated colonies formed. Colonies were picked and clonally expanded in G418/Puro selection media. The sequence of all generated constructs was verified and confirmed by restriction enzyme mapping and DNA sequencing.

#### RNA isolation and quantitative reverse-transcription PCR (qPCR)

Total RNA was isolated using the NucleoSpin RNA II kit with on-column rDNase treatment (Macherey–Nagel) and subsequently purified with NucleoSpin RNA Clean-up XS columns (Macherey–Nagel) according to the manufacturer's instructions. The concentration and quality of the purified RNA were determined using the NanoDrop 2000C (Thermo Scientific). One microgram of total RNA was reverse-transcribed using the Superscript II kit with oligo(dT)23 primers (Life Technologies). qPCRs were assembled using LightCycler 480 SYBR Green I Master mix (Roche) and cDNA-specific primers according to the manufacturer's instruction and run on the LightCycler 480 qPCR machine (Roche). Transcript levels were normalized to  $\beta$ -actin and/or *Gapdh* and compared to an untreated control sample. Samples were run in triplicate. Primer sequences are listed in Table EV6.

#### Immunoblotting and antibodies

For quantitative analysis of protein expression with immunoblotting, cells were washed with ice-cold PBS prior to lysis with TNTE lysis buffer (150 mM NaCl, 50 mM Tris–HCl, 1 mM EDTA, 1 mM phenylmethylsulfonyl fluoride (PMSF), 0.5% Triton X-100; pH 7.4) containing 1 $\times$  Complete protease inhibitors (Roche). Whole-cell lysates were centrifuged at 14,000 g and total protein concentration in the resultant supernatants was quantified using the Bradford assay. Twenty micrograms of total protein was loaded into each

well, resolved on 4–20% SDS–PAGE, transferred to nitrocellulose membranes, blocked with 5% skim milk in TBST (10 mM Tris–HCl, 100 mM NaCl, 0.1% Tween-20; pH 7.3), and probed with the primary antibodies overnight at 4°C with rocking. The following primary antibodies were used to detect proteins in whole-cell/subcellular lysates and/or IP lysates: mouse anti-FLAG antibody (1:1,000; M2, Sigma-Aldrich), rabbit anti-MKRN1 antibody (1:1,000; Abcam [ab72054]), rabbit anti-OCT3/4 (1:500; BD Transduction Laboratories), rabbit anti-PABP (1:1,000, Cell Signaling Technologies), mouse anti-IGF2BP1 (1:1,000; MBL International), mouse anti-HuR (1:1,000; 3A2, Santa Cruz), rabbit anti-cleaved caspase-3 (1:1,000; Cell Signaling Technologies), rabbit anti-cleaved PARP (1:1,000; Cell Signaling Technologies), mouse anti-p53 (1:1,000; 1C12, Cell Signaling Technologies), and mouse anti-GAPDH (1:5,000; Abcam). Following incubation with primary antibodies, blots were probed with the respective secondary antibodies (1:15,000): goat anti-mouse (H+L) 800 (Thermo Scientific) or goat anti-rabbit (H+L) Alexa Fluor 680 (Life Technologies) in the dark for 1 h at room temperature. Blots were imaged using the Odyssey Infrared Imager (Li-Cor), and bands corresponding to the expected size of the protein were quantified using the Odyssey 3.0 software.

#### Intracellular flow cytometry

OCT4 and MKRN1 protein expression profiling of single cells was analyzed by flow cytometry using anti-Oct3/4 antibody (BD Biosciences, 611203) and anti-MKRN1 antibody (Abcam, ab72054). Secondary antibodies included goat anti-mouse IgG (Alexa Fluor 555, Life Technologies) and goat anti-rabbit IgG (Alexa Fluor 488). Briefly, mESCs were grown on 10-cm gelatinized dishes for 72 h in +LIF, –LIF, or –LIF plus 100 nM RA. At the 72-h time point, cells were trypsinized to single-cell suspensions, fixed in 4% paraformaldehyde for 15 min, and permeabilized with 0.3% Triton X-100 in PBS at RT for 15 min. Cells were then incubated with primary antibody at 4°C for 30 min at 1:50 dilution, washed, and treated with secondary antibody at 4°C for 30 min at 1:100 dilution in the dark before analyzed by flow cytometry. As a negative control, cells were stained with appropriate secondary antibody only. Samples were run through using the LSRFortessa, and analyses were performed and collected using the BD FACSDiva software. OCT4-positive and OCT4-negative cells were gated based on single-colored controls. Mean fluorescent intensity of MKRN1 was quantified from the OCT4-positive and OCT4-negative fractions from each culture condition.

#### Immunofluorescence microscopy and high-content imaging analysis (HCA)

Cells were washed with PBS, fixed with 3.7% formaldehyde, permeabilized with 0.3% Triton X-100, and blocked with 5% goat serum and 1% bovine serum albumin in 0.3% Triton X-100 before the addition of the appropriate primary and secondary antibodies. Primary antibodies included the following: mouse anti-FLAG antibody (1:1,000, M2, Sigma-Aldrich), rabbit anti-MKRN1 antibody (1:2,000, Abcam), mouse anti-OCT3/4 (1:200, BD Transduction Laboratories), and mouse anti-HuR (1:1,000; 3A2, Santa Cruz). Cells were incubated with primary antibodies in blocking solution overnight at 4°C, washed three times, and incubated with the

appropriate secondary antibodies: goat anti-mouse and/or goat anti-rabbit Alexa Fluors 488 and 555 (1:500, Life Technologies), in the dark for 1 h at room temperature. Individual nuclei were stained with Hoechst 33342 dye (Life Technologies).

Epifluorescence microscopy images were captured on either a Leica DMIRE2 inverted microscope, or the Thermo Cellomics Arrayscan II HCA Reader with a Hamamatsu ORCA-ER CCD C4742-95 camera. For HCA, cells were imaged at 5× magnification and object identification was performed using the Target Activation algorithm for OCT4, or the Cell Health Profiling algorithm for MKRN1 (available as part of the Cellomics v2 Discovery Toolbox). Briefly, individual cells were identified through counterstaining of nuclei with Hoechst 33342. OCT4 protein intensities were quantified in the second channel to determine the undifferentiated (OCT4<sup>+</sup>) and committed (OCT4<sup>-</sup>) subpopulations as previously described [15,16,76]. MKRN1 protein expression was quantified in the third channel through dilation of the nuclear mask. Average pixel intensities within the masked regions were ln-transformed and plotted as histograms. Threshold values for MKRN1 were set as the median ln average immunofluorescence intensity in the undifferentiated population cultured for 72 h +LIF. Differential protein expression was assessed by shifts in pixel intensities away from the median threshold values.

#### Affinity purification and tandem mass spectrometry analysis

FLAG:MKRN1 and FLAG vector control (FLAG:Ctrl) ESC clones were expanded in feeder-free culture conditions. For the detection of putative MKRN1 ubiquitinated substrate proteins by mass spectrometry analysis, 10<sup>8</sup> ESCs were treated with 20 μM MG132 or with vehicle (DMSO) 5 h prior to lysis. For all immunoprecipitation experiments, cells were washed with ice-cold PBS prior to lysis with TNTE lysis buffer containing 1× Complete protease inhibitors (Roche) followed by gentle rocking at 4°C for 20 min. Whole-cell lysates were centrifuged at 14,000 g, and total protein in the resultant supernatants was quantified using the Bradford assay. For each IP, an equal amount of total protein was used between each sample; generally, 1.5–2.0 mg of total protein was used for each IP. Prior to the IP, lysates were pre-cleared with 150 μl of a 20% slurry of protein G-Sepharose beads (GE Healthcare) while agitating at 4°C for 1 h. Subsequently, cleared lysates were immunoprecipitated with 60 μl of a 50% slurry anti-FLAG antibody conjugated to agarose beads (M2, Sigma-Aldrich) while agitating at 4°C for 1 h. Following the IP, beads were washed extensively in TNTE wash buffer (150 mM NaCl, 50 mM Tris-HCl, 1 mM EDTA, 0.1% Triton X-100; pH 7.4) and either trypsinized in preparation for mass spectrometry analysis or boiled in 2× sample buffer supplemented with 100 mM dithiothreitol (DTT) and resolved on 4–20% SDS-PAGE for immunoblot analysis. For identification of RNA-dependent and RNA-independent associations, following anti-FLAG immunoprecipitation of 4 mg total protein from either FLAG:MKRN1 or FLAG:Ctrl ESC lysates, anti-FLAG beads were washed five times in 1 ml NT2 buffer (50 mM Tris-HCl pH 7.4, 150 mM NaCl, 1 mM MgCl<sub>2</sub>, 0.1% Nonidet P-40). Following the fifth wash, the anti-FLAG beads suspension was split into two fresh tubes such that half of the beads were digested with 200 μg/ml RNase A (Sigma-Aldrich; R4642) in –/– PBS for 1 h while rocking at RT and the other half of the beads were left to rock in –/–PBS only. Elutants from RNase A-treated and untreated beads were collected, while proteins that remained

bound to anti-FLAG beads were washed twice in NT2 buffer prior to Western blot or mass spectrometry analysis.

For mass spectrometry analysis, FLAG:MKRN1-associated proteins were identified with liquid chromatography tandem mass spectrometry (LC-MS/MS) on an LTQ mass spectrometer (Thermo Scientific), programmed for data-dependent MS/MS acquisition (one precursor ion scan, followed by three consecutive product ion scans). The RAW files generated by XCalibur (Thermo Scientific) were converted into DTA or mzXML files and searched using SEQUEST against 16,253 mouse proteins from the UniProt/Swiss-Prot database. An empirical false discovery rate of 3.0% was determined using a reverse decoy peptide sequence [77]. Enriched proteins in FLAG:MKRN1 AP-MS replicates were determined on the basis of total spectral counts relative to FLAG:Ctrl AP-MS replicates using a pairwise *t*-test adjusted for multiple testing with the Benjamini–Hochberg correction method. Adjusted *P*-value of < 0.05 was used to identify enriched proteins between FLAG:MKRN1 and FLAG:Ctrl samples.

#### Functional classification of the FLAG:MKRN1 AP-MS data set

Functional annotations for enriched proteins in the FLAG:MKRN1 AP-MS data set was performed in DAVID [78] and visualized with the Enrichment Map Plugin v1.2 [46] in Cytoscape using the following parameters (*P*-value cutoff = 0.001; FDR *Q*-value cutoff = 0.1; Jaccard coefficient = 0.25). Enriched proteins sets are represented as nodes (red circles) connected by edges (green lines). Edges connect nodes with common proteins within the gene sets. The thickness of the edges denotes the degree of gene set overlap between connected nodes. The node size is proportional to the number of proteins in the gene set. Groups of functionally related gene sets are circled in gray and labeled in blue. Select nodes that connect several distinct functionally related gene sets (hubs) are labeled in black.

#### Cross-linking immunoprecipitation (CLIP) and autoradiography

The protocol was adapted from [79,80]. FLAG:MKRN1 and FLAG:Ctrl ESC clones were expanded on 15-cm dishes in feeder-free culture conditions in mESC media. Cells were washed with cold PBS and irradiated on ice with UV light in a Stratalinker (254 nm) once at 400 mJ/cm<sup>2</sup> and a second time at 200 mJ/cm<sup>2</sup>. Cells were then scraped, centrifuged at 600 g for 5 min, and resuspended in 650 μl PXL lysis buffer (PBS without Ca<sup>2+</sup> and Mg<sup>2+</sup>, 0.1% SDS, 0.5% NP-40 and 1:50 RNase-free RQ1 DNase, and 1:100 RNase OUT). RNase A (70194Y) was diluted as indicated in 1× PXL buffer, and 10 μl of this solution was added to ESC lysates. Lysates were briefly digested with RNase A for 5 min at 37°C and diluted to 1.5 ml in PXL and cell debris was pelleted at 300 g (5 min). ESC lysates were then incubated with anti-FLAG M2 magnetic beads (Sigma-Aldrich) or Protein G Dynabeads® (Life Technologies) pre-armed with 10 μg of anti-IgG<sub>1</sub> antibodies overnight at 4°C while rotating. Beads were washed four times with 500 μl 1× PXL and twice with PNK buffer (50 mM Tris-HCl (pH 7.5), 0.5% NP-40, 5 mM MgCl<sub>2</sub>). RNA was then labeled by resuspending beads in 40 μl of PNK mix (4 μl 10× PNK reaction buffer B, 2 μl (10 U) of T4 PNK (Fermentas), 0.5–1.0 μl [γ-<sup>32</sup>P]ATP (10 mCi/ml), 1 μl RNase inhibitor and 32 μl water) and incubating for 15 min at 37°C at 800 rpm on a

Thermomixer. Beads were subsequently washed three times with ice-cold 1× PXL (gentle pipetting up and down) and twice with ice-cold PNK buffer. Radiolabeled RNA–protein complexes were eluted from beads with 40 µl NuPAGE LDS buffer diluted (1:3) in PNK buffer, by mixing at 1,000 rpm at 75°C for 10 min in a Thermomixer. Protein-bound RNAs were loaded onto 4–12% Bis-Tris NuPAGE gel (Life Technologies) and transferred to nitrocellulose membrane for autoradiography or immunoblot analysis with anti-MKRN1 antibodies (1:1,000).

### Ribonucleoprotein immunoprecipitation microarray (RIP-chip) and RIP-qPCR

RIPs were performed using a modified procedure described previously [81]. RIP was carried out using 4 mg of total protein from bulk FLAG:MKRN1 or FLAG:Ctrl ESC lysates. Cells were lysed with ice-cold polysome lysis buffer (100 mM KCl, 5 mM MgCl<sub>2</sub>, 100 nM ZnCl<sub>2</sub>, 10 mM HEPES pH 7.4, 1% Nonidet P-40, 100 U/ml RNaseOUT, 1 mM DTT, 1 mM PMSF, 400 µM vanadyl ribonucleoside, complexes and 1× Roche Complete protease inhibitors). RIP was carried out for 1 h at 4°C in 1 ml of NT2 buffer (50 mM Tris-HCl pH 7.4, 150 mM NaCl, 1 mM MgCl<sub>2</sub>, 100 nM ZnCl<sub>2</sub>, 0.1% Nonidet P-40, 100 U/ml RNaseOUT, 0.2 mM PMSF, and 1× Roche Complete protease inhibitors) using 100 µl of a 50% slurry of Protein G Dynabeads® (Life Technologies) pre-armed with 10 µg of anti-FLAG, or anti-IgG<sub>1</sub> antibodies. Just prior to initiating the immunoprecipitation, one-tenth of the volume of each RIP lysate was saved for extraction of “input” RNA. For purification of MKRN1-associated mRNAs, a FLAG RIP was performed from FLAG:MKRN1 ESC lysates. To control for spurious interactions, two control RIPs were performed in parallel: (i) a FLAG RIP from FLAG:Ctrl ESC lysates and (ii) an isotype antibody control RIP from the FLAG:MKRN1 ESC lysates. Following the immunoprecipitation, beads were washed 6× in 1 ml NT2 buffer. After the final wash of the beads, RIP and input samples were treated with 30 µg of proteinase K for 30 min at 55°C to elute RNA from the beads. RIP and input RNA was extracted with ultra pure phenol–chloroform–isoamyl alcohol (25:24:1; Life Technologies) followed by LiCl ethanol RNA precipitation. RIP and input RNA was treated with DNase I (Life Technologies) according to the manufacturer’s instructions and subsequently ethanol precipitated. Purified RIP and input RNA was quantified using the RNA Pico Chip Kit (Agilent) on the Agilent 2100 BioAnalyzer. Ten nanograms of RIP or input RNA was used to generate cDNA used in subsequent RIP-chip or RIP-qPCR analyses.

For RIP-chip analysis, the Nugen Ovation Pico WTA system was used to convert 10 ng of RIP and input RNA to double-stranded cDNA, to amplified sense-strand cDNA, and finally to fragmented, biotinylated cDNA. About 2.5 µg biotinylated cDNA was hybridized to Affymetrix Mouse Gene 1.0 ST microarrays following the manufacturer’s instructions. Hybridization, washes, and staining were performed using Affymetrix protocols on a FS450 fluidics station. Scanning was performed using the Affymetrix GeneChip Scanner 30007G. CEL files generated by the Affymetrix GeneChip Command Console (v3.0.1.1229) were quantile normalized in Genespring GX v11 using PLIER16. The log<sub>2</sub> normalized signal values were then filtered to remove entities that show signal values in the bottom 20<sup>th</sup> percentile across all samples. To be considered mRNA targets of

MKRN1, probes from anti-FLAG FLAG:MKRN1 RIPs had to be at least two times greater than the signal from corresponding probes from the two control RIPs: anti-FLAG FLAG:Ctrl RIP and anti-IgG<sub>1</sub> FLAG:MKRN1 RIP.

For RIP-qPCR analyses, 10 ng of RIP and input RNA was converted to cDNA with Superscript II kit and oligo(dT)<sub>23</sub> primers (Life Technologies). qPCRs were assembled as previously described. Fold enrichment of transcripts from the anti-FLAG:MKRN1 RIPs was calculated relative to the two control RIPs: anti-FLAG FLAG:Ctrl RIP and anti-IgG<sub>1</sub> FLAG:MKRN1 RIP. Nine transcripts that were not identified as enriched in the FLAG:MKRN1 RIP data set served as a negative control group to calculate a threshold value by which putative MKRN1 target mRNAs (transcripts that were identified as enriched from RIP:chip) were compared. The threshold value (1.78-fold enrichment) was calculated as two standard deviations from the mean fold enrichment of the negative control group.

### Transient transfection of pLKO.1 shRNA puro constructs in ESCs

A total of  $1.7 \times 10^5$  ESCs/well were seeded in a 12-well gelatinized plate in mESC media. Following 48 h, cells were transfected overnight with 2 µg of the respective supercoiled plasmid: pLKO.1 shGFP control and pLKO.1 shMKRN1 (same shRNA sequences as described above) using Lipofectamine 2000 (Life Technologies) according to the manufacturer’s protocol in mESC media (LIF + serum; no puromycin selection). The following day, the media were replaced with 1 ml of fresh mESC media. Twenty-four hours later, mESC media were replaced with mESC media supplemented with 2 µg/ml puromycin (selection media). Selection media were changed daily for 4 days at which point only puromycin-resistant cells remained. At this time point (6 days post-transfection; 4 days post-puromycin selection), cells were either fixed with 3.7% formaldehyde and stained for alkaline phosphatase activity [82], or lysed for RNA extraction.

### Microarray expression analysis

Total RNA harvested from transiently transfected ESCs was isolated using the Macherey–Nagel RNeasy columns with on-column DNase I treatment according to the manufacturer’s instructions. Each sample of eluted total RNA was then run through Macherey–Nagel RNA clean-up XS columns clean-up kit according to the manufacturer’s instructions. The concentration and quality of the purified RNA were determined using both the NanoDrop and the RNA Nano Chip Kit (Agilent) on the Agilent 2100 BioAnalyzer. A total of 500 ng of high-quality total RNA obtained from four independent transient transfection experiments was converted to fragmented, biotinylated cDNA (Ambion WT Expression kit), and hybridized to the Affymetrix Mouse Gene 1.0 ST microarrays. Hybridizations of four biological replicates for the shGFP- and shMKRN1-transfected ESC populations were performed. Hybridization, washes, and staining were performed using Affymetrix products and equipment. Scanning was performed using the Affymetrix GeneChip Scanner 3000.

Using the Bioconductor package (v.2.8) in R language environment, CEL files that contained raw signal intensity values were preprocessed and normalized using RMA to correct for background intensity. The expression data were transformed into log<sub>2</sub> values

and were fit on multiple linear models each probe across available matrix. The contrast design matrix between the shGFP- and the shMKRN1-transfected samples was applied to assess differential expression. Empirical Bayes statistics was applied to shrink the probe-wise sample variances toward a common value, which employed moderated *t*-statistics test and the moderated *F*-statistic tests analogous to conventional ANOVA except moderation of residual mean squares and residual degrees of freedom between probes. The *P*-value that corresponded to the moderated *t*-statistics was obtained. The Benjamini–Hochberg correction method was used to determine the FDR and obtain adjusted *P*-values. Adjusted *P*-value of < 0.05 was used to identify differentially expressed transcripts between shGFP- and shMKRN1-transfected ESC populations. Transcripts whose abundance was affected more than 1.3-fold (linear range) in either direction were considered up- or downregulated. Transcripts with modest changes in expression values of less than 1.3-fold (linear range), in either direction, were considered non-regulated.

#### Integrative genomic analysis of RIP data set with microarray data

To characterize the expression profiles of the FLAG:MKRN1 RIP data set, the 3,192 unique transcripts comprising this data set were mapped onto microarray expression data derived from undifferentiated ESC populations. Three different microarray data sets [11,16] and shGFP control microarray data from this study (Accession Number: GSE59394) were mapped separately against the FLAG:MKRN1 RIP data set. Mapping and analysis was done with custom code in Bioconductor package (v.2.8) in R language environment. Independent analyses with each of the three microarray data sets demonstrated an enrichment of low-abundance transcripts in the FLAG:MKRN1 RIP data set; however, due to differences in coverage between each microarray data set and the FLAG:MKRN1 RIP data set, the number of unique MKRN1-associated transcripts that mapped onto each microarray data set varied: Ivanova *et al* (40.1% coverage), Walker *et al* (79.1% coverage) and this study (99.8% coverage). Thus for subsequent bioinformatic analysis, including binning of the MKRN1–mRNA network, the FLAG:MKRN1 RIP data set was mapped against the microarray expression data generated in this study (Accession Number: GSE59394), which was performed on the same platform as RIP-chip experiments (Affymetrix Mouse Gene 1.0 ST microarrays).

Determination of global expression profiles for transcripts in the mESC transcriptome and the FLAG:MKRN1 RIP data set involved extracting raw expression matrix values from available microarray data derived from undifferentiated ESCs for 1,102,500 probes across multiple replicates. Average value for each probe was calculated and non-normalized (raw) values were plotted on a log-scale histogram as previously described [10]. RMA-normalized expression values corresponding to transcripts in the ESC transcriptome and the unfiltered MKRN1 RIP data set were parsed, averaged, and plotted on the log-scale histogram. Transcripts from each subset were grouped into the three bins with respect to their expression in undifferentiated ESCs: low bin (expression values between 1 and 100), a middle bin (expression values between 100 and 1,000), and a high bin (expression values between 1,000 and 10,000). The distribution of 3,187 out of 3,192 enriched transcripts in the FLAG:MKRN1 RIP data set was compared to the distribution

of 20,388 non-redundant transcripts in the ESC transcriptome. Transcripts in the lowest bin (expression values between 1 and 100) were considered background and filtered from the FLAG:MKRN1 RIP data set to yield a filtered MKRN1–mRNA network of 1,870 unique transcripts.

#### Functional classification of the MKRN1–mRNA network

Gene-enrichment analysis for the 1,870 enriched transcripts in the MKRN1–mRNA network was performed in DAVID [78] and visualized with Enrichment Map Plugin v1.2 [46] in Cytoscape using the following parameters (*P*-value cutoff = 0.005; FDR *Q*-value cutoff = 0.1; Jaccard coefficient = 0.25). Enriched gene sets are represented as nodes (red circles) connected by edges (green lines). Edges connect nodes with common transcripts within gene sets. The thickness of the edges indicates the degree of overlap in transcripts between the connected nodes. The node size is proportional to the number of transcripts in the gene set. Groups of functionally related gene sets are circled in gray and labeled in blue. Nodes that connect several functionally related gene sets (hubs) are labeled in black.

#### Fractionation of cellular compartments

A total of  $10^8$  MKRN1 knockdown (shMKRN1) or shGFP control ESCs were resuspended in PBS, washed (500 g, 5 min) with 5 ml 0.25 M sucrose solution pH 7.2, and resuspended in 1 ml 0.25 M sucrose containing ribonuclease inhibitor (1 mM ribonucleoside vanadyl, Sigma-Aldrich). Cell membranes were gently disrupted by nitrogen cavitation (25 pounds per square inch, 8 min) achieving disruption of 85% of cells. Intact cells were eliminated by centrifugation at 2,000 g (5 min). The supernatant was divided into two aliquots, and 20 mM EDTA was added to one aliquot. Both aliquots were incubated at 37°C for 10 min. Both aliquots were then centrifuged at 17,000 g (12 min). The pellets containing endoplasmic reticulum membranes were collected for qPCR and immunoblot analysis while the supernatant was centrifuged at 100,000 g in a TLA-100.3 rotor (Beckman) for 16 min to eliminate smaller organelles and vesicles. The resultant supernatant, representing the soluble cytoplasmic fraction, was recovered for qPCR and immunoblot analysis. RNA was isolated from ER-enriched and soluble cytoplasmic fractions with TRIzol (Life Technologies) according to the manufacturer's protocol and subsequently ethanol precipitated to remove contaminants from the purified RNA. cDNA was generated from 1.5 µg ER-enriched or soluble RNA isolated from EDTA-treated and untreated lysates. cDNA was subsequently used for qPCR analysis on the LightCycler 480 qPCR machine as previously described. For each transcript, unnormalized expression values in the ER-enriched fraction were reported relative to unnormalized expression values in the soluble fraction for both EDTA-treated and untreated lysates. To determine whether the depletion of MKRN1 affected the distribution of mRNAs between the ER-enriched and cytoplasmic fraction, unnormalized ER-enriched/soluble expression values quantified from the two MKRN1 knockdown and shGFP control ESC clones were grouped and averaged such that the mean value of shGFP and MKRN1 knockdown ER-enriched/soluble expression values was plotted for EDTA-treated and untreated lysates.

### Immunoblot validation of subcellular fractionation technique

To confirm the efficiency of subcellular fractionation and EDTA treatment to dissociate ribosomes, EDTA-treated and untreated subcellular fractions from MKRN1 knockdown and shGFP control ESC clones were subjected to immunoblot analysis with the following primary antibodies: rabbit anti-calnexin (1:1,000; Enzo Life Sciences), rabbit anti-PABP (1:1,000; Cell Signaling Technologies), rabbit anti-MOV10 (1:1,000; Bethyl Laboratories), anti-histone H3K27-me3 (1:1,000; Abcam), and rabbit anti-MKRN1 antibody (1:1,000; Abcam). Immunoblot analysis verified that the ER luminal protein marker, calnexin, was uniquely detected in ER-enriched fractions and not visible in soluble (cytoplasmic). Moreover, immunoblotting for the nuclear marker, H3K27-me3, confirmed that nuclear proteins were absent from the ER-enriched and soluble fractions. The effectiveness of EDTA treatment to dissociate mRNPs from membrane-bound ribosome was gauged by immunoblotting for mRNP protein markers: PABP and the RNA helicase MOV10. Immunoblotting for MKRN1 confirmed its depletion exclusively in MKRN1 knockdown ESC lysates, and its subcellular localization in undifferentiated ESCs represented by shGFP control lysates.

### Induction of stress granules and confocal fluorescence microscopy

A total of  $10^6$  ESCs (R1, FLAG:Ctrl, FLAG:MKRN1, shGFP, or shMKRN1) were seeded on sterilized, 0.1% gelatin-coated glass coverslips (Corning; No. 1 22 mm sq) and cultured for 48 h in mESC media. To induce stress granule formation, ESCs were cultured in mESC media with 1 mM sodium arsenite (Sigma-Aldrich) or 10  $\mu$ M thapsigargin (Sigma-Aldrich) for 1 h. Then, cells were fixed in 3.7% formaldehyde and permeabilized with 0.3% Triton X-100/PBS. Cells were incubated in blocking solution (5% horse serum, 1% BSA in 0.3% Triton X-100 in PBS) for 1 h at RT. Cells were incubated with primary antibodies diluted in blocking solution overnight at 4°C. Primary antibodies included the following: mouse anti-FLAG antibody (1:1,000, M2; Sigma-Aldrich), rabbit anti-MKRN1 antibody (1:2,000; Abcam), mouse anti-OCT3/4 (1:200; BD Transduction Laboratories), mouse anti-HuR (1:1,000; 3A2, Santa Cruz), goat anti-TIAR (1:1,000; Santa Cruz), and rabbit anti-G3BP (1:200; Sigma-Aldrich). After washing, cells were incubated with donkey anti-mouse/anti-rabbit/anti-goat (H+L) secondary antibodies coupled to Alexa Fluors 488/555/647 (1:5,000; Life Technologies) in the dark for 1 h at RT. DNA was visualized using Hoechst 33342 (Life Technologies). After washing, cells were mounted onto glass slides using Immuno Fluore mounting medium (ICN Biomedicals). Images were acquired at 60 $\times$  magnification by spinning-disk confocal microscopy (Olympus ix81 inverted microscope, Yokogawa scan head and Hamamatsu EM-CCD 9100-13 camera). Image acquisition and analysis were performed with Volocity (v5.4; PerkinElmer) and compiled using Adobe Photoshop software.

### Induction of environmental and genotoxic stress-induced apoptosis

Apoptosis was induced in 70% confluent ESC populations using stress granule-inducing and non-stress granule-inducing stress. For stress granule-inducing stress, ESCs were treated for 30 min with 1 mM NaAsO<sub>2</sub> (Sigma-Aldrich) followed by a 4 h recovery period in

mESC media. Non-stress granule-inducing genotoxic stress was induced with 0.5  $\mu$ M adriamycin (ADR) (Sigma-Aldrich) treatment for 6 h. Following the respective treatment, floating and adherent cells were harvested, washed in ice-cold PBS, and lysed with TNTE buffer for immunoblot analysis.

### Accession numbers

Microarray array expression data and RIP-chip data sets have been deposited in the Gene Expression Omnibus (GEO) database under Accession Number GSE59394. The mass spectrometry proteomics data have been deposited to the ProteomeXchange Consortium via the PRIDE partner repository with the data set identifiers PXD001191 and PXD001291.

**Expanded View** for this article is available online:

<http://embor.embopress.org>

### Acknowledgements

We thank James Ellis, Jens Lykke-Andersen, Jason Moffat for reagents and Peter Zandstra, Quaid Morris, Lynn Megeney, Emily Walker, Kamal Garcha, Gareth Palidwor, Carol Perez-Iratxeta, and Andrey Shukalyuk for expert advice. This work was supported by Canadian Institutes for Health Research grants (MOP-89910 & EPS-129130) and a Natural Sciences and Engineering Research Council grant (RGPIN 293170-11) to WLS. PAC was supported by CIHR Banting and Best CGS Doctoral Research Award. RLC was funded in part by the Government of Ontario Ministry of Economic Development and Innovation for the Ontario Research Fund supporting the International Regulome Consortium. WLS is funded by a Tier 1 Canada Research Chair in Integrative Stem Cell Biology.

### Author contributions

PAC and RLC designed and performed experiments, analyzed and interpreted data, and wrote the manuscript. PST, JBO, HuG, JLW, and AE assisted with the AP-MS analyses. CJP, RMT, and TJP performed bioinformatic analysis. SAT advised RIP-chip studies. HoG and DG executed subcellular fractionation and CLIP experiments. ZC, SD, CC, and WYC confirmed findings by independently repeating experiments. WLS guided all experiments, interpreted data, and wrote the manuscript. All authors contributed to the edits.

### Conflict of interest

The authors declare that they have no conflict of interest.

### References

- Maeda T, Lee MJ, Palczewska G, Marsili S, Tesar PJ, Palczewski K, Takahashi M, Maeda A (2013) Retinal pigmented epithelial cells obtained from human induced pluripotent stem cells possess functional visual cycle enzymes in vitro and in vivo. *J Biol Chem* 288: 34484–34493
- Schwartz SD, Hubschman JP, Heilwell G, Franco-Cardenas V, Pan CK, Ostrick RM, Mickunas E, Gay R, Klimanskaya I, Lanza R et al (2012) Embryonic stem cell trials for macular degeneration: a preliminary report. *Lancet* 379: 713–720
- Evans MJ, Kaufman MH (1981) Establishment in culture of pluripotential cells from mouse embryos. *Nature* 292: 154–156
- Martin GR (1981) Isolation of a pluripotent cell line from early mouse embryos cultured in medium conditioned by teratocarcinoma stem cells. *Proc Natl Acad Sci USA* 78: 7634–7638

5. Thomson JA, Itskovitz-Eldor J, Shapiro SS, Waknitz MA, Swiergiel JJ, Marshall VS, Jones JM (1998) Embryonic stem cell lines derived from human blastocysts. *Science* 282: 1145–1147
6. Takahashi K, Yamanaka S (2006) Induction of pluripotent stem cells from mouse embryonic and adult fibroblast cultures by defined factors. *Cell* 126: 663–676
7. Yu J, Vodyanik MA, Smuga-Otto K, Antosiewicz-Bourget J, Frane JL, Tian S, Nie J, Jonsdottir GA, Ruotti V, Stewart R et al (2007) Induced pluripotent stem cell lines derived from human somatic cells. *Science* 318: 1917–1920
8. Takahashi K, Tanabe K, Ohnuki M, Narita M, Ichisaka T, Tomoda K, Yamanaka S (2007) Induction of pluripotent stem cells from adult human fibroblasts by defined factors. *Cell* 131: 861–872
9. Boyer LA, Lee TI, Cole MF, Johnstone SE, Levine SS, Zucker JP, Guenther MG, Kumar RM, Murray HL, Jenner RG et al (2005) Core transcriptional regulatory circuitry in human embryonic stem cells. *Cell* 122: 947–956
10. Chen X, Xu H, Yuan P, Fang F, Huss M, Vega VB, Wong E, Orlov YL, Zhang W, Jiang J et al (2008) Integration of external signaling pathways with the core transcriptional network in embryonic stem cells. *Cell* 133: 1106–1117
11. Ivanova N, Dobrin R, Lu R, Kotenko I, Levorse J, DeCoste C, Schafer X, Lun Y, Lemischka IR (2006) Dissecting self-renewal in stem cells with RNA interference. *Nature* 442: 533–538
12. Kim J, Chu J, Shen X, Wang J, Orkin SH (2008) An extended transcriptional network for pluripotency of embryonic stem cells. *Cell* 132: 1049–1061
13. Loh YH, Wu Q, Chew JL, Vega VB, Zhang W, Chen X, Bourque G, George J, Leong B, Liu J et al (2006) The Oct4 and Nanog transcription network regulates pluripotency in mouse embryonic stem cells. *Nat Genet* 38: 431–440
14. Marson A, Levine SS, Cole MF, Frampton GM, Brambrink T, Johnstone S, Guenther MG, Johnston WK, Wernig M, Newman J et al (2008) Connecting microRNA genes to the core transcriptional regulatory circuitry of embryonic stem cells. *Cell* 134: 521–533
15. Walker E, Chang WY, Hunkapiller J, Cagney G, Garcha K, Torchia J, Krogan NJ, Reiter JF, Stanford WL (2010) Polycomb-like 2 associates with PRC2 and regulates transcriptional networks during mouse embryonic stem cell self-renewal and differentiation. *Cell Stem Cell* 6: 153–166
16. Walker E, Ohishi M, Davey RE, Zhang W, Cassar PA, Tanaka TS, Der SD, Morris Q, Hughes TR, Zandstra PW et al (2007) Prediction and testing of novel transcriptional networks regulating embryonic stem cell self-renewal and commitment. *Cell Stem Cell* 1: 71–86
17. Tichy ED, Stambrook PJ (2008) DNA repair in murine embryonic stem cells and differentiated cells. *Exp Cell Res* 314: 1929–1936
18. Matoba R, Niwa H, Masui S, Ohtsuka S, Carter MG, Sharov AA, Ko MS (2006) Dissecting Oct3/4-regulated gene networks in embryonic stem cells by expression profiling. *PLoS ONE* 1: e26
19. Gray TA, Hernandez L, Carey AH, Schaldach MA, Smithwick MJ, Rus K, Marshall Graves JA, Stewart CL, Nicholls RD (2000) The ancient source of a distinct gene family encoding proteins featuring RING and C(3)H zinc-finger motifs with abundant expression in developing brain and nervous system. *Genomics* 66: 76–86
20. Ko A, Shin JY, Seo J, Lee KD, Lee EW, Lee MS, Lee HW, Choi IJ, Jeong JS, Chun KH et al (2012) Acceleration of gastric tumorigenesis through MKRN1-mediated posttranslational regulation of p14ARF. *J Natl Cancer Inst* 104: 1660–1672
21. Kim JH, Park S-M, Kang MR, Oh S-Y, Lee TH, Muller MT, Chung IK (2005) Ubiquitin ligase MKRN1 modulates telomere length homeostasis through a proteolysis of hTERT. *Genes Dev* 19: 776–781
22. Ko A, Lee E-W, Yeh J-Y, Yang M-R, Oh W, Moon J-S, Song J (2010) MKRN1 induces degradation of West Nile virus capsid protein by functioning as an E3 ligase. *J Virol* 84: 426–436
23. Lee EW, Kim JH, Ahn YH, Seo J, Ko A, Jeong M, Kim SJ, Ro JY, Park KM, Lee HW et al (2012) Ubiquitination and degradation of the FADD adaptor protein regulate death receptor-mediated apoptosis and necroptosis. *Nat Commun* 3: 978
24. Lee EW, Lee M-S, Camus S, Ghim J, Yang M-R, Oh W, Ha N-C, Lane DP, Song J (2009) Differential regulation of p53 and p21 by MKRN1 E3 ligase controls cell cycle arrest and apoptosis. *EMBO J* 28: 2100–2113
25. Salvatico J, Kim JH, Chung IK, Muller MT (2010) Differentiation linked regulation of telomerase activity by Makorin-1. *Mol Cell Biochem* 342: 241–250
26. Miroci H, Schob C, Kindler S, Ölschläger-Schütt J, Fehr S, Jungenitz T, Schwarzacher SW, Bagni C, Mohr E (2012) Makorin ring zinc finger protein 1 (MKRN1), a novel poly(A)-binding protein-interacting protein, stimulates translation in nerve cells. *J Biol Chem* 287: 1322–1334
27. Cano F, Miranda-Saavedra D, Lehner Paul J (2010) RNA-binding E3 ubiquitin ligases: novel players in nucleic acid regulation. *Biochem Soc Trans* 38: 1621
28. Hirotsune S, Yoshida N, Chen A, Garrett L, Sugiyama F, Takahashi S, Yagami K-i, Wynshaw-Boris A, Yoshiki A (2003) An expressed pseudogene regulates the messenger-RNA stability of its homologous coding gene. *Nature* 423: 91–96
29. Omwancha J, Zhou X-F, Chen S-Y, Baslan T, Fisher CJ, Zheng Z, Cai C, Shemshedini L (2006) Makorin RING finger protein 1 (MKRN1) has negative and positive effects on RNA polymerase II-dependent transcription. *Endocrine* 29: 363–373
30. Mellacheruvu D, Wright Z, Couzens AL, Lambert JP, St-Denis NA, Li T, Miteva YV, Hauri S, Sardi ME, Low TY et al (2013) The CRAPome: a contaminant repository for affinity purification-mass spectrometry data. *Nat Meth* 10: 730–736
31. Kedersha NL, Gupta M, Li W, Miller I, Anderson P (1999) RNA-binding proteins TIA-1 and TIAR link the phosphorylation of eIF-2 alpha to the assembly of mammalian stress granules. *J Cell Biol* 147: 1431–1442
32. Stöhr N, Lederer M, Reinke C, Meyer S, Hatzfeld M, Singer RH, Hüttelmaier S (2006) ZBP1 regulates mRNA stability during cellular stress. *J Cell Biol* 175: 527–534
33. Solomon S, Xu Y, Wang B, David M, Schubert P, Kennedy D, Schrader J (2007) Distinct Structural Features of Caprin-1 Mediate Its Interaction with G3BP-1 and Its Induction of Phosphorylation of Eukaryotic Translation Initiation Factor 2, Entry to Cytoplasmic Stress Granules, and Selective Interaction with a Subset of mRNAs. *Mol Cell Biol* 27: 2324–2342
34. Tourrière H, Chebli K, Zekri L, Courselaud B, Blanchard JM, Bertrand E, Tazi J (2003) The RasGAP-associated endoribonuclease G3BP assembles stress granules. *J Cell Biol* 160: 823–831
35. Kedersha N, Chen S, Gilks N, Li W, Miller IJ, Stahl J, Anderson P (2002) Evidence that ternary complex (eIF2-GTP-tRNA(i)(Met))-deficient preinitiation complexes are core constituents of mammalian stress granules. *Mol Biol Cell* 13: 195–210
36. Gilks N, Kedersha N, Ayodele M, Shen L, Stoecklin G, Dember LM, Anderson P (2004) Stress granule assembly is mediated by prion-like aggregation of TIA-1. *Mol Biol Cell* 15: 5383–5398
37. Mazroui R, Sukarieh R, Bordeleau M-E, Kaufman RJ, Northcote P, Tanaka J, Gallouzi I, Pelletier J (2006) Inhibition of ribosome recruitment induces stress granule formation independently of eukaryotic initiation factor 2alpha phosphorylation. *Mol Biol Cell* 17: 4212–4219

38. Mazroui R, Di Marco S, Kaufman RJ, Gallouzi I-E (2007) Inhibition of the ubiquitin-proteasome system induces stress granule formation. *Mol Biol Cell* 18: 2603–2618
39. Mokas S, Mills JR, Garreau C, Fournier M-J, Robert F, Arya P, Kaufman RJ, Pelletier J, Mazroui R (2009) Uncoupling stress granule assembly and translation initiation inhibition. *Mol Biol Cell* 20: 2673–2683
40. Peng JC, Valouev A, Swigut T, Zhang J, Zhao Y, Sidow A, Wysocka J (2009) Jarid2/Jumonji coordinates control of PRC2 enzymatic activity and target gene occupancy in pluripotent cells. *Cell* 139: 1290–1302
41. Boyer LA, Plath K, Zeitlinger J, Brambrink T, Medeiros LA, Lee TI, Levine SS, Wernig M, Tajonar A, Ray MK et al (2006) Polycomb complexes repress developmental regulators in murine embryonic stem cells. *Nature* 441: 349–353
42. Pasini D, Cloos PA, Walfridsson J, Olsson L, Bukowski JP, Johansen JV, Bak M, Tommerup N, Rappsilber J, Helin K (2010) JARID2 regulates binding of the Polycomb repressive complex 2 to target genes in ES cells. *Nature* 464: 306–310
43. Meissner A, Mikkelsen TS, Gu H, Wernig M, Hanna J, Sivachenko A, Zhang X, Bernstein BE, Nusbaum C, Jaffe DB et al (2008) Genome-scale DNA methylation maps of pluripotent and differentiated cells. *Nature* 454: 766–770
44. Mikkelsen TS, Ku M, Jaffe DB, Issac B, Lieberman E, Giannoukos G, Alvarez P, Brockman W, Kim TK, Koche RP et al (2007) Genome-wide maps of chromatin state in pluripotent and lineage-committed cells. *Nature* 448: 553–560
45. Li G, Margueron R, Ku M, Chambon P, Bernstein BE, Reinberg D (2010) Jarid2 and PRC2, partners in regulating gene expression. *Genes Dev* 24: 368–380
46. Merico D, Isserlin R, Stueker O, Emili A, Bader GD (2010) Enrichment map: a network-based method for gene-set enrichment visualization and interpretation. *PLoS ONE* 5: e13984
47. Pyhtila B, Zheng T, Lager PJ, Keene JD, Reedy MC, Nicchitta CV (2008) Signal sequence- and translation-independent mRNA localization to the endoplasmic reticulum. *RNA* 14: 445–453
48. Ivanov VN, Wen G, Hei TK (2013) Sodium arsenite exposure inhibits AKT and Stat3 activation, suppresses self-renewal and induces apoptotic death of embryonic stem cells. *Apoptosis* 18: 188–200
49. Galbán S, Kuwano Y, Pullmann R Jr, Martindale JL, Kim HH, Lal A, Abdelmohsen K, Yang X, Dang Y, Liu JO et al (2008) RNA-binding proteins HuR and PTB promote the translation of hypoxia-inducible factor 1alpha. *Mol Cell Biol* 28: 93–107
50. Arimoto K, Fukuda H, Imajoh-Ohmi S, Saito H, Takekawa M (2008) Formation of stress granules inhibits apoptosis by suppressing stress-responsive MAPK pathways. *Nat Cell Biol* 10: 1324–1332
51. Mazan-Mamczarz K, Hagner PR, Zhang Y, Dai B, Lehrmann E, Becker KG, Keene JD, Gorospe M, Liu Z, Gartenhaus RB (2011) ATM regulates a DNA damage response posttranscriptional RNA operon in lymphocytes. *Blood* 117: 2441–2450
52. Anderson P, Kedersha N (2009) Stress granules. *Curr Biol* 19: R397–R398
53. Aladjem MI, Spike BT, Rodewald LW, Hope TJ, Klemm M, Jaenisch R, Wahl GM (1998) ES cells do not activate p53-dependent stress responses and undergo p53-independent apoptosis in response to DNA damage. *Curr Biol* 8: 145–155
54. Lee K-H, Li M, Michalowski AM, Zhang X, Liao H, Chen L, Xu Y, Wu X, Huang J (2010) A genomewide study identifies the Wnt signaling pathway as a major target of p53 in murine embryonic stem cells. *Proc Natl Acad Sci USA* 107: 69–74
55. Lin T, Chao C, Si S, Mazur SJ, Murphy ME, Appella E, Xu Y (2005) p53 induces differentiation of mouse embryonic stem cells by suppressing Nanog expression. *Nat Cell Biol* 7: 165–171
56. Vinuesa CG, Cook MC, Angelucci C, Athanasopoulos V, Rui L, Hill KM, Yu D, Domaschitz H, Whittle B, Lambe T et al (2005) A RING-type ubiquitin ligase family member required to repress follicular helper T cells and autoimmunity. *Nature* 435: 452–458
57. Yu D, Tan AH, Hu X, Athanasopoulos V, Simpson N, Silva DG, Hutloff A, Giles KM, Leedman PJ, Lam KP et al (2007) Roquin represses autoimmunity by limiting inducible T-cell co-stimulator messenger RNA. *Nature* 450: 299–303
58. Buchet-Poyau K, Courchet J, Le Hir H, Séraphin B, Scoazec J-Y, Duret L, Domon-Dell C, Freund J-N, Billaud M (2007) Identification and characterization of human Mex-3 proteins, a novel family of evolutionarily conserved RNA-binding proteins differentially localized to processing bodies. *Nucleic Acids Res* 35: 1289–1300
59. Piao X, Zhang X, Wu L, Belasco JG (2010) CCR4-NOT deadenylates mRNA associated with RNA-induced silencing complexes in human cells. *Mol Cell Biol* 30: 1486–1494
60. Castello A, Fischer B, Eichelbaum K, Horos R, Beckmann BM, Strein C, Davey NE, Humphreys DT, Preiss T, Steinmetz LM et al (2012) Insights into RNA biology from an atlas of mammalian mRNA-binding proteins. *Cell* 149: 1393–1406
61. Kwon SC, Yi H, Eichelbaum K, Fohr S, Fischer B, You KT, Castello A, Krijgsveld J, Hentze MW, Kim VN (2013) The RNA-binding protein - repertoire of embryonic stem cells. *Nat Struct Mol Biol* 20: 1122–1130
62. Cho J, Chang H, Kwon SC, Kim B, Kim Y, Choe J, Ha M, Kim YK, Kim VN (2012) LIN28A is a suppressor of ER-associated translation in embryonic stem cells. *Cell* 151: 765–777
63. Lebedeva S, Jens M, Theil K, Schwanhäusser B, Selbach M, Landthaler M, Rajewsky N (2011) Transcriptome-wide analysis of regulatory interactions of the RNA-binding protein HuR. *Mol Cell* 43: 340–352
64. Jønson L, Vikesaa J, Krogh A, Nielsen LK, Hansen TV, Borup R, Johnsen AH, Christiansen J, Nielsen FC (2007) Molecular composition of IMP1 ribonucleoprotein granules. *Mol Cell Proteomics* 6: 798–811
65. Evdokimova V, Ruzanov P, Anglesio MS, Sorokin AV, Ovchinnikov LP, Buckley J, Triche TJ, Sonenberg N, Sorensen PHB (2006) Akt-mediated YB-1 phosphorylation activates translation of silent mRNA species. *Mol Cell Biol* 26: 277–292
66. Hafner M, Landthaler M, Burger L, Khorshid M, Hausser J, Berninger P, Rothballer A, Ascano M Jr, Jungkamp AC, Munschauer M et al (2010) Transcriptome-wide identification of RNA-binding protein and microRNA target sites by PAR-CLIP. *Cell* 141: 129–141
67. Mukherjee N, Corcoran DL, Nusbaum JD, Reid DW, Georgiev S, Hafner M, Ascano M Jr, Tuschl T, Ohler U, Keene JD (2011) Integrative regulatory mapping indicates that the RNA-binding protein HuR couples pre-mRNA processing and mRNA stability. *Mol Cell* 43: 327–339
68. López de Silanes I, Zhan M, Lal A, Yang X, Gorospe M (2004) Identification of a target RNA motif for RNA-binding protein HuR. *Proc Natl Acad Sci USA* 101: 2987–2992
69. Mukherjee N, Lager PJ, Friedersdorf MB, Thompson MA, Keene JD (2009) Coordinated posttranscriptional mRNA population dynamics during T-cell activation. *Mol Syst Biol* 5: 288
70. Sheth U, Parker R (2003) Decapping and decay of messenger RNA occur in cytoplasmic processing bodies. *Science* 300: 805–808

71. Stead E, White J, Faast R, Conn S, Goldstone S, Rathjen J, Dhingra U, Rathjen P, Walker D, Dalton S (2002) Pluripotent cell division cycles are driven by ectopic Cdk2, cyclin A/E and E2F activities. *Oncogene* 21: 8320–8333
72. Li H, Collado M, Villasante A, Strati K, Ortega S, Cañamero M, Blasco MA, Serrano M (2009) The Ink4/Arf locus is a barrier for iPS cell reprogramming. *Nature* 460: 1136–1139
73. Hirao A, Kong YY, Matsuoka S, Wakeham A, Ruland J, Yoshida H, Liu D, Elledge SJ, Mak TW (2000) DNA damage-induced activation of p53 by the checkpoint kinase Chk2. *Science* 287: 1824–1827
74. Hong Y, Stambrook PJ (2004) Restoration of an absent G1 arrest and protection from apoptosis in embryonic stem cells after ionizing radiation. *Proc Natl Acad Sci USA* 101: 14443–14448
75. Moffat J, Grueneberg DA, Yang X, Kim SY, Kloepfer AM, Hinkle G, Piqani B, Eisenhaure TM, Luo B, Grenier JK et al (2006) A lentiviral RNAi library for human and mouse genes applied to an arrayed viral high-content screen. *Cell* 124: 1283–1298
76. Davey RE, Zandstra PW (2006) Spatial organization of embryonic stem cell responsiveness to autocrine gp130 ligands reveals an autoregulatory stem cell niche. *Stem Cells* 24: 2538–2548
77. Elias JE, Gygi SP (2007) Target-decoy search strategy for increased confidence in large-scale protein identifications by mass spectrometry. *Nat Meth* 4: 207–214
78. Huang DW, Sherman BT, Lempicki RA (2009) Systematic and integrative analysis of large gene lists using DAVID bioinformatics resources. *Nat Protoc* 4: 44–57
79. Chi SW, Zang JB, Mele A, Darnell RB (2009) Argonaute HITS-CLIP decodes microRNA-mRNA interaction maps. *Nature* 460: 479–486
80. Murigneux V, Saulière J, Roest Crollius H, Le Hir H (2013) Transcriptome-wide identification of RNA binding sites by CLIP-seq. *Methods* 63: 32–40
81. Baroni TE, Chittur SV, George AD, Tenenbaum SA (2008) Advances in RIP-chip analysis : RNA-binding protein immunoprecipitation-microarray profiling. *Methods Mol Biol* 419: 93–108
82. Pease S, Braghetta P, Gearing D, Grail D, Williams RL (1990) Isolation of embryonic stem (ES) cells in media supplemented with recombinant leukemia inhibitory factor (LIF). *Dev Biol* 141: 344–352



**License:** This is an open access article under the terms of the Creative Commons Attribution-NonCommercial-NoDerivs 4.0 License, which permits use and distribution in any medium, provided the original work is properly cited, the use is non-commercial and no modifications or adaptations are made.